Projection of the gravitational dynamics on a subspace of probability distributions: Curl-free Gaussian *Ansatz*

Patrick Valageas

Institut de Physique Théorique, Université Paris-Saclay,
CEA, CNRS, F-91191 Gif-sur-Yvette Cedex, France

We present a new approach to model the gravitational dynamics of large-scale structures. Instead of solving the equations of motion up to a finite perturbative order or building phenomenological models, we follow the evolution of the probability distribution of the displacement and velocity fields within an approximation subspace. Keeping the exact equations of motion with their full nonlinearity, this provides a nonperturbative scheme that goes beyond shell crossing. Focusing on the simplest case of a curl-free Gaussian *Ansatz* for the displacement and velocity fields, we find that truncations of the power spectra on nonlinear scales directly arise from the equations of motion. This leads to a truncated Zeldovich approximation for the density power spectrum, but with a truncation that is not set *a priori* and with different power spectra for the displacement and velocity fields. The positivity of their autopower spectra also follows from the equations of motion. Although the density power spectrum is only recovered up to a smooth drift on baryon acoustic oscillation (BAO) scales, the predicted density correlation function agrees with numerical simulations within 2% from BAO scales down to $7h^{-1}$ Mpc at $z \geq 0.35$, without any free parameter. Thus, this parameter-free extension of the Zeldovich approximation is not competitive with other schemes for the power spectrum, but it provides a good prediction for the correlation function. However, the improvement over the standard Zeldovich approximation remains rather modest. This means that including non-Gaussianities will be essential to significantly improve analytical predictions within this general framework.

I. INTRODUCTION

The large-scale structures that we observe in the current Universe and at low redshifts, i.e., the cosmic web, its filaments, galaxies, and clusters of galaxies, and Lyman-α absorption clouds, have emerged from the amplification by gravitational instability of small primordial perturbations. In the standard inflation scenario, these were generated by quantum fluctuations during the inflationary epoch. Next, once these density perturbations reach the nonlinear regime and form astrophysical objects such as galaxies or x-ray clusters, baryonic physics comes into play through heating and cooling processes, star formation, feedback from active galactic nuclei (AGN), etc. Therefore, the measurements of these large-scale structures provide key probes of the primordial mechanisms generating the initial seeds of these large-scale structures, of the underlying cosmological model (e.g., the amount of dark matter and dark energy) that affects the growth rate of the density fluctuations at all redshifts, and of the astrophysical processes associated with various objects (e.g., the bias of the tracers of the matter density field). More specifically, the baryon acoustic oscillations (BAOs) of the matter or galaxy power spectra, which correspond to a peak at about $110h^{-1}$ Mpc in the correlation functions, are a robust signature of the acoustic oscillations in the baryon-photon fluid before recombination that are also seen in the cosmic microwave background [1]. This provides a standard ruler that is able to constrain the low-redshift expansion of the Universe and the standard Λ cold dark matter (Λ-CDM) cosmological scenario [2]. Distortions of the images of background galaxies by the fluctuations of the gravitational potential along the lines of sight (weak gravitational lensing) also probe the total matter density fluctuations and provide direct constraints on the cosmological scenarios [3]. This has provided the motivation for several galaxy surveys in the last decades or the near future, such as the Baryon Oscillation Spectroscopic Survey [4], the WiggleZ Dark Energy Survey [5], the Dark Energy Spectroscopic Instrument [6], Euclid [7], or the Large Synoptic Survey Telescope [8].

The formation of these large-scale structures is often studied with numerical simulations, which can tackle highly nonlinear scales and also include various baryonic effects, such as star formation and feedback from AGN, if they include an hydrodynamic description for the gas in addition to the N-body codes that are adequate for CDM. However, it remains desirable to develop analytic or semianalytic methods. On large scales, they provide efficient tools that are more practical than numerical

simulations to explore a large parameter space. On a qualitative level, they also help to understand how different parameters or alternative theories (e.g., models of dark matter and dark energy or modified-gravity scenarios) affect the cosmological structures.

The standard analytical approach to study gravitational clustering in the late Universe is the standard perturbation theory (SPT) [9,10]. There, one writes the equations of motion in Eulerian space for the matter density and velocity fields, $\rho(\mathbf{x}, t)$ and $\mathbf{v}(\mathbf{x}, t)$, that is, the continuity and Euler equations, supplemented by the Poisson equation for the gravitational force. These equations being nonlinear (quadratic), one writes a perturbative expansion in powers of the primordial fluctuations and solves for the density and velocity fields up to some finite order. One can also employ various partial resummation schemes [11–14]. Finally, assuming Gaussian initial conditions, one takes the Gaussian average of products of these fields to compute the density and velocity polyspectra or n-point correlations. Going to second or third order in the linear power spectrum P_L improves the agreement with numerical simulations on large scales, as compared with the linear theory. However, the accuracy does not keep improving at higher orders and this scheme cannot reach nonlinear scales, even if all perturbative diagrams were resummed [15–18]. Indeed, the Euler equation itself is only an approximation that neglects shell crossing, where different streams coexist at a given location and give rise to nonzero velocity dispersion and vorticity [16,19,20].

A method to handle this problem is to explicitly consider coarse-grained equations of motion [21]. Another recent approach is the effective field theory (EFT) of large-scale structures [22,23]. Following methods devised in other fields where the equations of motion, or the Lagrangians, are not exactly known, one derives low-energy effective actions that are based on the symmetries of the problem, by taking into account all possible operators up to some order in a derivative expansion (for instance). For the cosmological dynamics, one considers a large-scale effective theory, taking into account all operators up to some order over the wave number k. In practice, this adds new counterterms to the SPT diagrams, which should capture the impact on large scales of small-scale nonperturbative processes, like shell crossing. The coefficients of these new terms cannot be derived and need to be fitted to numerical simulations. However, once these parameters have been set by fitting a few quantities, such as the power spectrum at a given scale, once can compute other statistical quantities. Thus, this framework remains predictive [24]. An advantage of this approach is that it can also handle baryons and biased tracers, such as galaxies, where indeed the equations of motion are not explicitly known or too complex to be of any use (e.g., one cannot include all astrophysical processes associated with star formation) [25–27]. Then, an effective approach is unavoidable. In practice, EFT schemes usually assume a curl-free velocity field and neglect the generation of vorticity by small-scale nonlinearities, so that they do not include all possible nonlinear effects. But this is expected to be a small effect on large scales and could be added to the formalism.

On the other hand, if we only consider dark matter, that is, if we neglect baryonic physics, the equations of motion are exactly known and given by Newton's (or Einstein's) gravity. Then, the traditional approach to handle shell crossing is to work in Lagrangian space, where we follow the trajectories of particles [28–37]. Then, the fundamental object is the displacement field $\mathbf{\Psi}(\mathbf{q}, t)$ and nothing peculiar appears at shell crossing. A disadvantage of this method is that one eventually needs to compute the statistics of the density field from the displacement field. This is a highly nonlinear transformation that leads to practical difficulties for many-point polyspectra or correlation functions. An alternative to this Lagrangian route is to go from the hydrodynamical equations, associated with the density and velocity fields, to the Vlasov equation, associated with the phase-space distribution $f(\mathbf{x}, \mathbf{v}, t)$. This provides an exact Eulerian-space description of the gravitational dynamics [38,39]. However, this leads to seven-dimensional fields, which makes computations very heavy and time consuming. Another recent alternative is to replace the hydrodynamical equations by the Schrödinger equation, which in some regime can provide an approximation to the Vlasov equation [40,41].

Another level of distinction between the different analytical approaches is whether they work with the equations of motion or directly with statistical quantities. The popular methods above work at the level of the equations of motion. There, one computes an approximation for $\rho(\mathbf{x}, t)$ in terms of the initial condition $\delta_{L0}(\mathbf{x})$, determined by the growing mode of the linear density contrast. Next, statistical quantities such as the power spectrum are obtained by taking the Gaussian average over products of such nonlinear functionals. Another approach is to first write the evolution equations satisfied by those statistical quantities and next solve them with some approximation scheme [42–44]. This typically leads to infinite series of equations that relate n- and $(n + 1)$-point correlation functions or polyspectra, as in the Bogoliubov-Born-Green-Kirkwood-Yvon (BBGKY) hierarchy [45]. Alternatively, one can work with the probability distribution functional of the fields [46] or the generating functional of the correlation functions [12,37,47]. An advantage of this approach is that such statistical quantities satisfy symmetries (e.g., translation invariance) that are not obeyed by individual realizations of the random fields, which can simplify some expressions. However, computations become cumbersome when going beyond three-point correlations.

In this paper, we present a new approach to follow the gravitational dynamics of large-scale structures. In contrast with most previous schemes, we wish to build a scheme

that is meaningful from large to small scales, hence going beyond perturbative treatments, and does not introduce free parameters that require fitting to numerical simulations. To handle shell crossings, we adopt a Lagrangian framework [in principle, we could also opt for the phase-space distribution $f(\mathbf{x}, \mathbf{v}, t)$]. We also work at the level of the probability distribution $\mathcal{P}(\mathbf{\Psi}, \mathbf{v}, t)$ of the displacement and velocity fields, instead of trying to solve the dynamics of individual realizations. Then, we propose to follow the progress of gravitational clustering by "projecting" the dynamics onto a subspace of trial distributions $\mathcal{P}$. This idea is an extension of the standard procedure to estimate the minimum of a nonlinear cost functional $S[\varphi(x)]$. There, one can expand φ over a finite basis, $\varphi = \sum_i a_i \psi_i$, which defines a subspace of possible functions φ, and look for the minimum of $S(\{a_i\})$. However, instead of a minimization problem, we use the equations of motion to follow the evolution of $\mathcal{P}(\mathbf{\Psi}, \mathbf{v}, t)$ within the lower-dimensional subspace of trial distributions $\{\mathcal{P}\}_{\text{trial}}$.

In this article, we consider the simplest case of Gaussian distributions $\{\mathcal{P}\}_{\text{trial}}$, which are fully defined by the displacement and velocity power spectra. Then, the evolution of $\mathcal{P}$ is determined by the equations of motion for these power spectra. As for the Eulerian-space BBGKY hierarchy [45], this is not a closed system, because these equations involve correlations with the gravitational force, which is a nonlinear functional of the displacement field. However, within the Gaussian *Ansatz* for $\mathcal{P}$ (or, more generally, given the form of $\mathcal{P}$ within the approximate subspace), we can exactly compute such correlations and close the system. In other words, in contrast to most approaches, we keep the exact equations of motion and only perform the truncation, or approximation, at the level of the distribution $\mathcal{P}$. This provides a nonperturbative scheme that can handle shell crossing and does not require parameters to be fitted by numerical simulations. The equations of motion themselves determine the parameters that enter the probability distribution $\mathcal{P}$, here the displacement and velocity power spectra. For the density field, this leads to a prediction that coincides with the truncated Zeldovich approximation. However, the truncation is not introduced by hand but arises from the equations of motion. Also, in contrast with the truncated Zeldovich approximation, the displacement and velocity power spectra are different.

Thus, although the Gaussian case studied in detail in this article is only a specific example of the more general method outlined above, it is also of interest by itself as a natural extension of the standard Zeldovich approximation without adding any free parameter. (As seen in the main sections, this is achieved by taking into account additional constraints, derived from the equations of motion, that uniquely determine the deviations from the usual Zeldovich approximation within the Gaussian *Ansatz*.)

This paper is organized as follows. In Sec. II, we recall the equations of motion for the displacement field and its probability distribution, as well as the expression of the gravitational force. In Sec. III, we give the evolution equations of the displacement and velocity power spectra, which provide constraints on the evolution of the distribution $\mathcal{P}$. Then, in Sec. IV, we present the simplest Gaussian *Ansatz* for the distribution $\mathcal{P}$ and derive its closure of the system of equations of motion. We briefly compare our approach with other analytical schemes in Sec. V. Then, in Sec. VI, we first present our numerical computations for the case of self-similar dynamics, with power-law linear power spectra in the Einstein–de Sitter cosmology. We turn to the realistic Λ-CDM cosmology in Sec. VII and conclude in Sec. VIII.

II. EQUATIONS OF MOTION

A. Lagrangian displacement field

In a Lagrangian framework, we describe the dynamics by following the comoving trajectories $\mathbf{x}(\mathbf{q}, t)$ of the particles, labeled by their initial comoving position $\mathbf{q}$. As usual, it is convenient to introduce the displacement $\mathbf{\Psi}(\mathbf{q}, t)$ so that the positions at time t read

$$\mathbf{x}(\mathbf{q}, t) = \mathbf{q} + \mathbf{\Psi}(\mathbf{q}, t). \tag{1}$$

Then, standard Lagrangian perturbation theory aims at computing the trajectories $\mathbf{x}(\mathbf{q}, t)$ as a perturbative expansion over powers of the displacement $\mathbf{\Psi}$ [29,31–33]. In the expanding Universe, the equation of motion of the gravitational dynamics reads

$$\ddot{\mathbf{\Psi}} + 2H\dot{\mathbf{\Psi}} = -\frac{\nabla_{\mathbf{x}}\Phi}{a^2}, \tag{2}$$

where the dot denotes the partial derivative with respect to time, $a(t)$ is the scale factor, $H = \dot{a}/a$ is the Hubble expansion rate, and Φ is the gravitational potential. Because we work with comoving coordinates, the background expansion has been subtracted and Φ is only sourced by the density perturbations $\rho - \bar{\rho}$, where $\bar{\rho}$ is the background density. Thus, Φ is given by the Poisson equation

$$\nabla_{\mathbf{x}}^2 \Phi = a^2 4\pi \mathcal{G}(\rho - \bar{\rho}), \tag{3}$$

where $\mathcal{G}$ is Newton's constant, and its explicit expression is often written as

$$\Phi(\mathbf{x}, t) = -a^2 \mathcal{G} \int d\mathbf{x}' \frac{\rho(\mathbf{x}') - \bar{\rho}}{|\mathbf{x}' - \mathbf{x}|}. \tag{4}$$

The background counterterm also corresponds to the well-known Jeans "swindle," which regularizes the infrared divergence of the gravitational force due to an infinite homogeneous background. As pointed out in [48–50], a more satisfactory expression is obtained by introducing a screening of the gravitational interaction with distance,

$$\Phi(\mathbf{x}, t) = -a^2 \mathcal{G} \int d\mathbf{x}' \rho(\mathbf{x}') \frac{e^{-\mu|\mathbf{x}'-\mathbf{x}|}}{|\mathbf{x}' - \mathbf{x}|}, \quad (5)$$

and taking the limit $\mu \to 0$ at the end of the computations. Indeed, an homogeneous background gives a finite constant contribution to the potential Φ, which does not contribute to the gravitational force $\mathbf{F} = -\nabla_{\mathbf{x}}\Phi$. This corresponds to the screened Poisson equation,

$$\nabla_{\mathbf{x}}^2 \Phi - \mu^2 \Phi = a^2 4\pi \mathcal{G} \rho. \quad (6)$$

Solving this equation in Fourier space, we obtain at once

$$\Phi(\mathbf{x}, t) = -a^2 4\pi \mathcal{G} \int \frac{d\mathbf{x}' d\mathbf{k}}{(2\pi)^3} e^{i\mathbf{k}\cdot(\mathbf{x}-\mathbf{x}')} \frac{1}{k^2 + \mu^2} \rho(\mathbf{x}'). \quad (7)$$

This is simply Eq. (5) with the Fourier representation of the screened gravitational interaction.

A difficulty that one often encounters in Lagrangian perturbation theory is that the gravitational force $\nabla_{\mathbf{x}}\Phi$ in the equation of motion (2) is naturally written in Eulerian space $\mathbf{x}$, as in the Poisson equation (3) or the expression (5). Then, in the course of the perturbative computation, one may switch back and forth from Eulerian to Lagrangian space. In the standard Lagrangian perturbation theory [29,31–33], one takes the divergence of the equation of motion (2) with respect to $\mathbf{x}$, so as to use the Poisson equation to eliminate the gravitational potential in favor of the density. The latter is obtained from the conservation of matter as $\rho/\bar{\rho} = |\det(\partial \mathbf{q}/\partial \mathbf{x})|$. This leads to a nonlinear equation in Ψ, of cubic order in three dimensions [51]. It is often supplemented by the requirement of a curl-free Eulerian velocity field. This latter step is valid at all orders of Eulerian perturbation theory, but it is not exact because shell crossing generates a nonzero vorticity [19,20].

In this paper, we follow a different approach, as we do not take the divergence of the equation of motion (2). Instead, as in [37] we directly obtain the gravitational force from the explicit expression (7) of the gravitational potential in terms of the density field. Indeed, mass conservation allows us to derive a simple expression that only involves the Lagrangian trajectories. Before shell crossing we have $\rho(\mathbf{x})d\mathbf{x} = \bar{\rho}d\mathbf{q}$, while after shell crossing we need to sum over all streams. In both cases, the gravitational potential (7) is simply written as

$$\Phi(\mathbf{x}, t) = -a^2 4\pi \mathcal{G} \bar{\rho} \int \frac{d\mathbf{q}' d\mathbf{k}}{(2\pi)^3} e^{i\mathbf{k}\cdot[\mathbf{x}-\mathbf{x}(\mathbf{q}',t)]} \frac{1}{k^2 + \mu^2}. \quad (8)$$

Thus, instead of counting the mass in Eulerian space with the density field, we simply count the particles, labeled by the initial position $\mathbf{q}'$.

In the linear regime over the displacement field Ψ or the density perturbation $\delta = (\rho - \bar{\rho})/\bar{\rho}$, denoted by the subscript L, the linear growing mode is the curl-free displacement given in Fourier space by

$$\Psi_L(\mathbf{k}, t) = \frac{i\mathbf{k}}{k^2} \delta_L(\mathbf{k}, t), \qquad \delta_L(\mathbf{k}, t) = D_+(t)\delta_{L0}(\mathbf{k}). \quad (9)$$

The linear growing mode $D_+(t)$ is given by

$$\ddot{D}_+ + 2H\dot{D}_+ = 4\pi \mathcal{G}\bar{\rho}D_+, \quad (10)$$

and at early times in the matter era we have $D_+(t) \propto a(t) \propto t^{2/3}$. It is convenient to use $\eta = \ln D_+(t)$ as the time coordinate. Then, the equation of motion (2) reads

$$\frac{\partial^2 \Psi}{\partial \eta^2} + \left(\frac{3\Omega_m}{2f^2} - 1\right)\frac{\partial \Psi}{\partial \eta} = \frac{3\Omega_m}{2f^2}\mathbf{F}, \quad (11)$$

where we introduced the linear growth rate $f(t)$,

$$f(t) = \frac{d \ln D_+}{d \ln a} = \frac{\dot{D}_+}{HD_+}, \quad (12)$$

and the gravitational force $\mathbf{F}(\mathbf{q}, \eta)$ on the particle $\mathbf{q}$ reads

$$\mathbf{F}(\mathbf{q}, \eta) = \int \frac{d\mathbf{q}' d\mathbf{k}}{(2\pi)^3} e^{i\mathbf{k}\cdot[\mathbf{x}(\mathbf{q})-\mathbf{x}(\mathbf{q}')]} \frac{i\mathbf{k}}{k^2 + \mu^2}. \quad (13)$$

As compared with the expression in [37], we have added the regularization factor μ^2. In this fashion, the equation of motion (11) is fully written in terms of the Lagrangian-space displacement field, at the price of a strong nonlinearity as the exponential generates terms at all orders in powers of Ψ. All the cosmological dependence is captured by the factors Ω_m/f^2. This factor remains close to unity at all redshifts and it is often approximated by unity in perturbative computations. This approximate symmetry can actually be used to derive approximate consistency relations that go beyond low-order perturbation theory [52,53].

B. Linear displacement field

We can check that the linear growing mode (9) is a solution of the linearized equation derived from Eq. (11). At linear order, the force reads

$$\mathbf{F}_L(\mathbf{q}) = \int \frac{d\mathbf{q}' d\mathbf{k}}{(2\pi)^3} e^{i\mathbf{k}\cdot(\mathbf{q}-\mathbf{q}')}[1 + i\mathbf{k}\cdot(\Psi_L - \Psi_L')]\frac{i\mathbf{k}}{k^2 + \mu^2}. \quad (14)$$

The terms $1 + i\mathbf{k}\cdot\Psi_L$, which do not depend on $\mathbf{q}'$, give a vanishing contribution as the integral over $\mathbf{q}'$ gives a Dirac factor $\delta_D(\mathbf{k})$. (Thus, we explicitly see how the background contribution vanishes thanks to the screening beyond distance $1/\mu$.) Substituting the linear expression (9) gives

$$\mathbf{F}_L(\mathbf{q}) = \int \frac{d\mathbf{q}' d\mathbf{k} d\mathbf{k}'}{(2\pi)^3} e^{i\mathbf{k}\cdot(\mathbf{q}-\mathbf{q}')+i\mathbf{k}'\cdot\mathbf{q}'} \frac{\mathbf{k}\cdot\mathbf{k}'}{k'^2}\delta_L(\mathbf{k}')\frac{i\mathbf{k}}{k^2 + \mu^2}. \quad (15)$$

The integration over $\mathbf{q}'$ gives the Dirac factor $\delta_D(\mathbf{k}' - \mathbf{k})$, and the integration over $\mathbf{k}'$ gives

$$\mathbf{F}_L(\mathbf{q}) = \int d\mathbf{k} \, e^{i\mathbf{k}\cdot\mathbf{q}} \frac{i\mathbf{k}}{k^2 + \mu^2} \delta_L(\mathbf{k}). \qquad (16)$$

Then, for $\mu \to 0$ we obtain $\mathbf{F}_L(\mathbf{q}) \to \mathbf{\Psi}_L(\mathbf{q})$ and we can see that $\mathbf{\Psi}_L$ is solution of Eq. (11), as $\mathbf{\Psi}_L(\mathbf{q},\eta) = e^\eta \mathbf{\Psi}_{L0}(\mathbf{q})$ and $\partial \mathbf{\Psi}_L / \partial \eta = \mathbf{\Psi}_L$.

C. Probability distribution

The second-order differential equation of motion (11) can be written as a system of two first-order differential equations if we introduce the velocity field $\mathbf{v}$,

$$\mathbf{v}(\mathbf{q},\eta) \equiv \frac{\partial \mathbf{\Psi}}{\partial \eta}. \qquad (17)$$

This gives the coupled first-order system

$$\frac{\partial \mathbf{\Psi}}{\partial \eta} = \mathbf{v}, \qquad (18)$$

$$\frac{\partial \mathbf{v}}{\partial \eta} + \left(\frac{3\Omega_m}{2f^2} - 1\right)\mathbf{v} = \frac{3\Omega_m}{2f^2}\mathbf{F}[\mathbf{\Psi}], \qquad (19)$$

where we made explicit that $\mathbf{F}$ is a functional of $\mathbf{\Psi}$.

The probability distribution functional $\mathcal{P}(\mathbf{\Psi},\mathbf{v};\eta)$ of the displacements and velocities obeys the continuity equation (see also [46] for the Eulerian-space probability distribution)

$$\frac{\partial \mathcal{P}}{\partial \eta} + \int d\mathbf{q} \left[\frac{\delta}{\delta \mathbf{\Psi}(\mathbf{q})} \left(\frac{\partial \mathbf{\Psi}}{\partial \eta} \mathcal{P} \right) + \frac{\delta}{\delta \mathbf{v}(\mathbf{q})} \left(\frac{\partial \mathbf{v}}{\partial \eta} \mathcal{P} \right) \right] = 0. \qquad (20)$$

As for the usual Liouville equation, it describes the conservation of probability in phase space, here the functional space $\{\mathbf{\Psi},\mathbf{v}\}$. Substituting the dynamical equations (18) and (19), we obtain a closed evolution equation for $\mathcal{P}(\mathbf{\Psi},\mathbf{v};\eta)$. The advantage of the evolution equation (20) is that it does not require keeping track of past history. In contrast, perturbative approaches based on the equation of motion (2), or its Eulerian counterparts for the density and velocity fields, generate an increasingly large number of integrations over past times as one goes to higher orders. Indeed, each new order involves one more integration over the time-dependent Green's function associated with the linearized equation of motion. To bypass this complication, we can attempt to solve directly the equation (20) for the distribution $\mathcal{P}$: from the (approximate) knowledge of $\mathcal{P}$ at a given time η we can derive the distribution at the next time step $\eta + \Delta\eta$, without needing the cross-correlations with earlier times. This is actually what numerical simulations do, advancing particles over one time step from their current positions and velocities.

In practice, we do not expect to find the exact solution of the nonlinear functional equation (20). One possibility is to look for a perturbative expansion of $\mathcal{P}$ around the Gaussian, which describes the linear regime. This is the method investigated in [46] for the probability distribution of the density and velocity fields in the Eulerian framework. In contrast, the main idea of this paper is to apply a nonperturbative method, by considering trial distributions and using the dynamical equation (20) to derive constraints that fully determine the free parameters of such *Ansätze*. The hope is that by considering a sequence of increasingly detailed and versatile *Ansätze*, each one satisfying the equation of motion (20) to the "best possible accuracy" within its class, we converge to the true distribution $\mathcal{P}$. This is similar to a standard minimization problem, where we look for the absolute minimum of a nonlinear cost functional $S[\varphi(x)]$. One method is to expand the function $\varphi(x)$ over a basis of orthonormal functions ψ_i, $\varphi = \sum_i a_i \psi_i$, which is truncated at some order N, and to minimize the associated cost function $S(\{a_i\})$. If the basis $\{\psi_i\}$ is well chosen, in favorable cases the sequence of approximations $\{\varphi_N\}$ will converge to the exact minimum.

However, our problem is more complex than this minimization problem, as we do not have a uniquely defined cost functional S. Thus, within a given class of trial distributions $\mathcal{P}$, it is not obvious how we select the "best" choice. Our approach will be to use the evolution equation (20) to derive a set of constraints satisfied by $\mathcal{P}$, choosing the simplest ones that we can build. Then, we determine $\mathcal{P}$ from a self-consistency condition, by requiring it satisfies this set of constraints. As we increase the complexity and versatility of $\mathcal{P}$, hence its number of free parameters, we can take into account an increasing number of constraints. For instance, if we intend to characterize the probability distribution by its moments, we can obtain from the evolution equation (20) an expression for the time derivative of each moment. Then, truncating at a finite order N, as in the Edgeworth expansion of a probability distribution around the Gaussian, we can determine the moments or cumulants up to order N from these N constraint equations. Here, we can see the ambiguity associated with this method. Although it is more natural to use the constraints derived from the time derivative of the moments of order one to N, to determine a distribution parametrized by its N first moments, in principle, we could have chosen the constraints derived from the time derivative of the moments of order p to $p - 1 + N$, for any p, or any other set of N constraints. The true distribution satisfies an infinite number of constraints, e.g., for all higher-order cumulants, and we can expect to improve the accuracy of our trial distributions by including an increasing number of constraints.

D. Density power spectrum

Assuming we have obtained the statistics of the displacement field $\mathbf{\Psi}$, we can obtain the statistics of the density field, as for the well-known Zeldovich approximation [28].

Indeed, as for Eq. (8), integrals over the density field in Eulerian space can be written as integrals over Lagrangian space, and we have

$$\delta(\mathbf{k}) = \int \frac{d\mathbf{x}}{(2\pi)^3} e^{-i\mathbf{k}\cdot\mathbf{x}} \delta(\mathbf{x}) \qquad (21)$$

$$= \int \frac{d\mathbf{q}}{(2\pi)^3} (e^{-i\mathbf{k}\cdot\mathbf{x}(\mathbf{q})} - e^{-i\mathbf{k}\cdot\mathbf{q}}). \qquad (22)$$

Defining the density power spectrum as

$$\langle \delta(\mathbf{k}_1)\delta(\mathbf{k}_2) \rangle = \delta_D(\mathbf{k}_1 + \mathbf{k}_2) P(k_1), \qquad (23)$$

this gives for $k > 0$ [54,55]

$$P(k) = \int \frac{d\mathbf{q}}{(2\pi)^3} \langle e^{i\mathbf{k}\cdot[\mathbf{x}(\mathbf{q})-\mathbf{x}(0)]} \rangle. \qquad (24)$$

This expression is exact, so that, in principle, no further approximation is needed to go from the displacement field Ψ to the density field. However, if Ψ is not Gaussian, the average in Eq. (24) may be difficult to compute. In particular, it involves the moments of Ψ at all orders.

III. CONSTRAINT EQUATIONS

As explained in the previous section, because we cannot fully solve Eq. (20) for the evolution of the probability distribution $\mathcal{P}(\Psi, \mathbf{v}; \eta)$, the approach we propose in this paper is to use the more limited information associated with constraint equations that are consequences of this evolution equation. The hope is that this reduction can make the problem tractable while retaining enough information to strongly constrain the final approximation. As we shall see in the next section, because we consider in this paper a Gaussian *Ansatz* for the probability distribution $\mathcal{P}(\Psi, \mathbf{v}; \eta)$, constraints associated with the displacement and velocity power spectra will be sufficient for our purpose. More precisely, let us define the divergences in Lagrangian space χ and θ of the displacement and velocity fields,

$$\chi(\mathbf{q}, \eta) = -\nabla_{\mathbf{q}} \cdot \Psi, \qquad \theta(\mathbf{q}, \eta) = -\nabla_{\mathbf{q}} \cdot \mathbf{v}. \quad (25)$$

Then, taking the divergence of the equations of motion (18) and (19), we obtain

$$\frac{\partial \chi}{\partial \eta} = \theta, \qquad (26)$$

$$\frac{\partial \theta}{\partial \eta} + \left(\frac{3\Omega_m}{2f^2} - 1\right)\theta = \frac{3\Omega_m}{2f^2}\zeta, \qquad (27)$$

where we introduced the divergence of the force in Lagrangian space,

$$\zeta(\mathbf{q}, \eta) = -\nabla_{\mathbf{q}} \cdot \mathbf{F}. \qquad (28)$$

From the equation of motion (26), we obtain for the time derivative of the equal-times product

$$\frac{\partial}{\partial \eta} \langle \chi_1 \chi_2 \rangle = \langle \theta_1 \chi_2 + \chi_1 \theta_2 \rangle, \qquad (29)$$

where $\chi_i = \chi(\mathbf{q}_i, \eta)$. This gives for the equal-times power spectrum $P_{\chi\chi}(k, \eta)$

$$\frac{\partial P_{\chi\chi}}{\partial \eta} = 2P_{\chi\theta}. \qquad (30)$$

In the same fashion, from Eqs. (26) and (27) we obtain

$$\frac{\partial P_{\chi\theta}}{\partial \eta} = P_{\theta\theta} + \left(1 - \frac{3\Omega_m}{2f^2}\right)P_{\chi\theta} + \frac{3\Omega_m}{2f^2}P_{\chi\zeta} \qquad (31)$$

and

$$\frac{\partial P_{\theta\theta}}{\partial \eta} = \left(2 - \frac{3\Omega_m}{f^2}\right)P_{\theta\theta} + \frac{3\Omega_m}{f^2}P_{\theta\zeta}. \qquad (32)$$

All equations written so far are exact. Of course, the problem is that the system (30)–(32) is not closed, as it involves the force cross-power spectra $P_{\chi\zeta}$ and $P_{\theta\zeta}$.

In the linear regime, we have seen from Eq. (16) that $\mathbf{F}_L = \Psi_L$. Therefore, $\zeta_L = \chi_L$ and we have

$$P_{L\chi\chi} = P_{L\chi\theta} = P_{L\chi\zeta} = P_{L\theta\theta} = P_{L\theta\zeta} = P_{L\zeta\zeta} = e^{2\eta}P_{L0}(k),$$

$$(33)$$

and we can check that this is a solution of the system (30)–(32).

In the nonlinear regime, to be able to use the system (30)–(32) we also need to express $P_{\chi\zeta}$ and $P_{\theta\zeta}$ in terms of $\{P_{\chi\chi}, P_{\chi\theta}, P_{\theta\theta}\}$. This is the point where our approximation scheme enters, as described in Sec. IV below for the case of a curl-free Gaussian *Ansatz*.

As noticed in the previous section, there is some freedom in the choice of the constraint equations, and instead of considering these two-point statistics, we could have chosen the constraints associated with the time derivatives of higher-order moments $\langle \chi^n \theta^m \rangle$ or more intricate nonlinear functionals. The constraints (30)–(32) have the advantage of simplicity and seem more natural to constrain a Gaussian *Ansatz*, such as the one presented in Sec. IV below.

IV. CURL-FREE GAUSSIAN *ANSATZ*

A. Definition of the *Ansatz*

To illustrate the method proposed in this paper, we consider the simplest *Ansatz* for the probability distribution $\mathcal{P}$: the curl-free Gaussian displacement field. Thus, we generalize the linear solution (9) by writing

$$\boldsymbol{\Psi}(\mathbf{k}) = \frac{i\mathbf{k}}{k^2}\chi(\mathbf{k}), \qquad \mathbf{v}(\mathbf{k}) = \frac{i\mathbf{k}}{k^2}\theta(\mathbf{k}), \qquad (34)$$

where χ and θ are the displacement and velocity divergences defined in Eq. (25), and we take χ and θ to be Gaussian scalar fields with zero mean.

Then, the power spectra $P_{\chi\chi}(k,\eta)$, $P_{\chi\theta}(k,\eta)$, and $P_{\theta\theta}(k,\eta)$ fully define the Gaussian probability distribution $\mathcal{P}(\boldsymbol{\Psi}, \mathbf{v}; \eta)$. This *Ansatz* goes beyond the linear regime in two manners: First, the power spectrum $P_{\chi\chi}$ can be different from the linear density power spectrum. Second, the spectra $P_{\chi\chi}(k,\eta)$, $P_{\chi\theta}(k,\eta)$, and $P_{\theta\theta}(k,\eta)$ can be different from one another. This means that this *Ansatz* is also more general than the Zeldovich approximation.

Let us briefly discuss this zero-mean Gaussian *Ansatz*. From the conservation of matter, the displacement $\boldsymbol{\Psi}$ and its divergence χ are related to the density contrast by

$$1 + \delta = \frac{\rho}{\bar{\rho}} = \left| \det\left(\frac{\partial\mathbf{q}}{\partial\mathbf{x}}\right) \right| = \left| \det\left(\frac{\partial\mathbf{x}}{\partial\mathbf{q}}\right) \right|^{-1}, \quad (35)$$

which also reads as

$$1 + \delta = \left| \det\left(1 + \frac{\partial\boldsymbol{\Psi}}{\partial\mathbf{q}}\right) \right|^{-1}. \quad (36)$$

In multistreaming regions, we need to sum over the different streams. In the linear regime, we can expand the determinant and obtain at linear order

$$\delta_L = -\mathrm{Tr}\left(\frac{\partial\boldsymbol{\Psi}_L}{\partial\mathbf{q}}\right) = -\nabla_{\mathbf{q}} \cdot \boldsymbol{\Psi}_L = \chi_L, \quad (37)$$

and we recover $\delta_L = \chi_L$ at linear order. On the other hand, in a one-dimensional system, we would have

$$\text{1D: } \delta = \sum_{\text{streams}} \left| \frac{\partial x}{\partial q} \right|^{-1} - 1 = \sum_{\text{streams}} \frac{1}{|1-\chi|} - 1. \quad (38)$$

As gravitational clustering develops, most particles fall inside virialized halos or nonlinear structures such as filaments. Then, the density contrast $\delta(\mathbf{q})$ evaluated in Lagrangian space is increasingly large and the statistical average, weighted by the number of particles, is dominated by these high-density regions. Therefore, the Lagrangian-space mean $\langle\delta\rangle_{\mathbf{q}}$ becomes large and positive, whereas the Eulerian-space mean $\langle\delta\rangle_{\mathbf{x}} = 0$ always remains zero because of mass conservation. Then, from the close relation between the density and the displacement divergence χ in the linear regime and in the 1D case, one may wonder whether $\chi(\mathbf{q})$ should also develop a nonzero mean in the nonlinear regime. However, one can see from the definition (25) that this is not the case. Indeed, approximating the derivative by a finite-difference ratio,

$$\chi(\mathbf{q}) \simeq -\sum_{i=1}^{3} \frac{\Psi_i(\mathbf{q} + \epsilon\mathbf{e}_i) - \Psi_i(\mathbf{q})}{\epsilon}, \quad (39)$$

where $\mathbf{e}_i$ are the three unit vectors that form the Cartesian basis of the 3D Lagrangian space, we directly obtain $\langle\chi\rangle = 0$ from $\langle\Psi_i\rangle = 0$. As this is valid for any ϵ, it also holds in the limit $\epsilon \to 0$ for the derivative (25). This property can be more easily understood in the 1D case, where

$$\text{1D: } \frac{\partial x}{\partial q} = 1 + \frac{\partial\Psi}{\partial q} = 1 - \chi. \quad (40)$$

For instance, let us consider the adhesion model [56], where particles do not cross but stick together after collisions to form halos of zero size and infinite density. Then, over the Lagrangian interval Δq associated with a halo of mass $\bar{\rho}\Delta q$, the particles have the same Eulerian coordinate $x(q) = x_i$, given by the position of the halo. Hence, they have $\psi = x_i - q, \frac{\partial\Psi}{\partial q} = -1$ and $\chi = 1$, which gives back an infinite density in agreement with (38). Thus, χ does not diverge as halo densities grow, but its typical value in Lagrangian space, as measured, for instance, by the median of its probability distribution, becomes nonzero and close to -1 in the 1D adhesion model. Nevertheless, its mean remains zero because as we move from one halo at x_1 to the next one at x_2 the displacement field jumps from $\psi = x_1 - q$ to $\psi = x_2 - q$. Such sudden jumps correspond to very large negative values of χ (to $-\infty$ in this adhesion model). These rare but very large negative values compensate the typical values at $\chi \simeq 1$, so that the mean remains zero, $\langle\chi\rangle_q = 0$. This can also be understood by integrating (40) over a large interval Δq,

$$\frac{1}{\Delta q}\int_0^{\Delta q} dq\chi = 1 - \int \frac{dq}{\Delta q}\frac{\partial x}{\partial q} = 1 - \frac{x(\Delta q) - x(0)}{\Delta q}. \quad (41)$$

If on large scales the relative fluctuations decay fast enough, that is, $|x(\Delta q) - x(0)| - \Delta q$ grows more slowly than Δq (typically it remains finite and of the order of the size of the largest nonlinear structures), for large Δq we obtain zero from the last equality in (41). By ergodicity, the vanishing of the spatial average (41) also means that the statistical average vanishes, $\langle\chi\rangle_q = 0$. Thus, $\langle\chi\rangle_q = 0$ is related to the conservation of volume. Even though particles do not remain homogeneously distributed and gather in high-density halos among large voids, their typical displacement is finite at any time (of the order of the nonlinear scale) and particles initially separated by a distance $\Delta\mathbf{q}$ much greater than the linear scale are still separated by a distance $\Delta\mathbf{x} \simeq \Delta\mathbf{q}$ in Eulerian space. This discussion also shows that a more realistic model than the Gaussian distribution for χ would be a highly skewed distribution on small nonlinear scales, with still a zero mean but an extended tail to negative values and a peak at finite

positive values that contains most of the probabilistic weight. However, in this exploratory paper, we focus on the Gaussian model.

Clearly, this Gaussian *Ansatz* allows us to close the system (30)–(32), because by its definition all statistical properties of the fields $\mathbf{\Psi}$ and $\mathbf{v}$ are determined by the power spectra $\{P_{\chi\chi}, P_{\chi\theta}, P_{\theta\theta}\}$. Then, the correlations $\langle\chi\zeta\rangle$ and $\langle\theta\zeta\rangle$ are also fully determined by these three power spectra, because the gravitational force is fully determined by the positions of the particles. Note that the divergence of the force ζ is not Gaussian, as it is a nonlinear functional of the displacement, but within our Gaussian *Ansatz* we only need the two-point spectra $P_{\chi\zeta}$ and $P_{\theta\zeta}$ to close the system. Then, once we have expressed $P_{\chi\zeta}$ and $P_{\theta\zeta}$ in terms of $\{P_{\chi\chi}, P_{\chi\theta}, P_{\theta\theta}\}$, we obtain a closed system that fully determines the evolution of the power spectra $\{P_{\chi\chi}, P_{\chi\theta}, P_{\theta\theta}\}$, given their initial conditions set by the linear regime (9),

$$\eta \to -\infty: \; P_{\chi\chi} = P_{\chi\theta} = P_{\theta\theta} = e^{2\eta} P_{L0}(k). \quad (42)$$

B. Force-displacement and force-velocity cross-power spectra

1. Damping factor $\lambda(k)$

To close the system (30)–(32) and compute the time evolution of the power spectra, hence of the Gaussian distribution $\mathcal{P}$, we need to compute the force-displacement and force-velocity spectra $P_{\chi\zeta}$ and $P_{\theta\zeta}$. To avoid the problems associated with the homogeneous background and to focus on the divergence ζ of the force, it is convenient to consider the quantity

$$C_{\chi\zeta}(Q) = -\langle\chi(\mathbf{q}_1)\int_{|\mathbf{q}_2-\mathbf{q}_1|=Q} dS_2 \mathbf{n}_2 \cdot \mathbf{F}(\mathbf{q}_2)\rangle. \quad (43)$$

The integral is the flux of the force through the sphere of radius Q, around the point $\mathbf{q}_1$ in Lagrangian space. Here $\mathbf{n}_2$ is the outward normal vector to the sphere S_2. Using the divergence theorem and Eq. (28), it only depends on the divergence ζ of the force and is written

$$C_{\chi\zeta}(Q) = \int_{|\mathbf{q}_2-\mathbf{q}_1|\leq Q} d\mathbf{q}_2\langle\chi(\mathbf{q}_1)\zeta(\mathbf{q}_2)\rangle. \quad (44)$$

Going to Fourier space, we obtain

$$C_{\chi\zeta}(Q) = (4\pi)^2 Q^2 \int_0^\infty dk k P_{\chi\zeta}(k) j_1(kQ), \quad (45)$$

which is a simple Hankel transform of the power spectrum $P_{\chi\zeta}$. Then, to derive $P_{\chi\zeta}$ we only need to compute $C_{\chi\zeta}(Q)$ from its definition (43), using the explicit expression (13) of the gravitational force. This reads

$$C_{\chi\zeta}(Q) = -iQ^2 \int d\Omega_2 \int \frac{d\mathbf{q}'d\mathbf{k}'}{(2\pi)^3} \frac{\mathbf{n}_2 \cdot \mathbf{k}'}{k'^2 + \mu^2}$$
$$\times \langle\chi(\mathbf{q}_1)e^{i\mathbf{k}'\cdot[\mathbf{x}(\mathbf{q}_2)-\mathbf{x}(\mathbf{q}')]}\rangle, \quad (46)$$

where $\mathbf{q}_2 = \mathbf{q}_1 + Q\mathbf{n}_2$. Using the general property that if φ and Φ are Gaussian fields of zero mean we have

$$\langle\varphi e^\Phi\rangle = \langle\varphi\Phi\rangle e^{\langle\Phi^2\rangle/2}, \quad (47)$$

we obtain

$$C_{\chi\zeta}(Q) = Q^2 \int d\Omega_2 \int \frac{d\mathbf{q}'d\mathbf{k}'}{(2\pi)^3} \frac{\mathbf{n}_2 \cdot \mathbf{k}'}{k'^2 + \mu^2} e^{i\mathbf{k}'\cdot(\mathbf{q}_2-\mathbf{q}')}$$
$$\times \langle\chi(\mathbf{q}_1)[\mathbf{k}' \cdot (\mathbf{\Psi}(\mathbf{q}_2) - \mathbf{\Psi}(\mathbf{q}'))]\rangle$$
$$\times e^{-\langle[\mathbf{k}'\cdot(\mathbf{\Psi}(\mathbf{q}_2)-\mathbf{\Psi}(\mathbf{q}'))]^2\rangle/2}. \quad (48)$$

Going to Fourier space, we obtain from Eq. (34)

$$\langle\chi(\mathbf{q}_1)\mathbf{\Psi}(\mathbf{q}_2)\rangle = -i\int d\mathbf{k}_1 \frac{\mathbf{k}_1}{k_1^2} e^{i\mathbf{k}_1\cdot(\mathbf{q}_1-\mathbf{q}_2)} P_{\chi\chi}(k_1), \quad (49)$$

and

$$\frac{1}{2}\langle[\mathbf{k}' \cdot (\mathbf{\Psi}(\mathbf{q}_2) - \mathbf{\Psi}(\mathbf{q}_1))]^2\rangle$$
$$= \int d\mathbf{k}'' P_{\chi\chi}(k'')$$
$$\times \left(\frac{\mathbf{k}' \cdot \mathbf{k}''}{k''^2}\right)^2 [1 - \cos(\mathbf{k}'' \cdot (\mathbf{q}_2 - \mathbf{q}_1))]. \quad (50)$$

With the change of variable $\mathbf{q}' = \mathbf{q}_2 - \mathbf{q}$, this gives

$$C_{\chi\zeta}(Q) = iQ^2 \int d\Omega_2 \int \frac{d\mathbf{q}d\mathbf{k}'d\mathbf{k}_1}{(2\pi)^3} \frac{\mathbf{n}_2 \cdot \mathbf{k}'}{k'^2 + \mu^2} \frac{\mathbf{k}' \cdot \mathbf{k}_1}{k_1^2}$$
$$\times P_{\chi\chi}(k_1)e^{-\int d\mathbf{k}'' P_{\chi\chi}(k'')[1-\cos(\mathbf{k}''\cdot\mathbf{q})](\mathbf{k}'\cdot\mathbf{k}'')^2/k''^4}$$
$$\times e^{i\mathbf{k}'\cdot\mathbf{q}-iQ\mathbf{n}_2\cdot\mathbf{k}_1}(e^{i\mathbf{k}_1\cdot\mathbf{q}} - 1). \quad (51)$$

Using the property

$$\int d\mathbf{\Omega}(\mathbf{n} \cdot \mathbf{k}_2)e^{iQ\mathbf{n}\cdot\mathbf{k}_1} = i4\pi \frac{\mathbf{k}_2 \cdot \mathbf{k}_1}{k_1} j_1(k_1 Q), \quad (52)$$

where $j_1(z)$ is the first-order spherical Bessel function, the integration over $\mathbf{\Omega}_2$ gives

$$C_{\chi\zeta}(Q) = 4\pi Q^2 \int \frac{d\mathbf{q}d\mathbf{k}'d\mathbf{k}_1}{(2\pi)^3} \frac{(\mathbf{k}' \cdot \mathbf{k}_1)^2}{(k'^2 + \mu^2)k_1^3} P_{\chi\chi}(k_1)$$
$$\times j_1(k_1 Q)e^{-\int d\mathbf{k}'' P_{\chi\chi}(k'')[1-\cos(\mathbf{k}''\cdot\mathbf{q})](\mathbf{k}'\cdot\mathbf{k}'')^2/k''^4}$$
$$\times e^{i\mathbf{k}'\cdot\mathbf{q}}(e^{i\mathbf{k}_1\cdot\mathbf{q}} - 1). \quad (53)$$

The integral over the angles of $\mathbf{q}$ and $\mathbf{k}'$ leaves a quantity that no longer depends on the direction of $\mathbf{k}_1$. Therefore, the comparison with Eq. (45) directly gives

$$P_{\chi\zeta}(k) = P_{\chi\chi}(k)\lambda(k), \tag{54}$$

with

$$\lambda(k) = \int \frac{d\mathbf{q}d\mathbf{k}'}{(2\pi)^3} \frac{(\mathbf{k}' \cdot \mathbf{k})^2}{(k'^2 + \mu^2)k^2} e^{i\mathbf{k}'\cdot\mathbf{q}}(e^{i\mathbf{k}\cdot\mathbf{q}} - 1)$$
$$\times e^{-\int d\mathbf{k}'' P_{\chi\chi}(k'')[1-\cos(k''\cdot\mathbf{q})](\mathbf{k}'\cdot\mathbf{k}'')^2/k''^4}. \tag{55}$$

Defining the quantities $\alpha(q)$ and $\beta(q)$ by

$$\alpha(q) = \frac{4\pi}{3} \int_0^\infty dk P_{\chi\chi}(k)[1 - j_0(kq) - j_2(kq)], \tag{56}$$

$$\beta(q) = 4\pi \int_0^\infty dk P_{\chi\chi}(k) j_2(kq), \tag{57}$$

we have

$$\int d\mathbf{k}'' P_{\chi\chi}(k'') \frac{(\mathbf{k} \cdot \mathbf{k}'')^2}{k''^4}[1 - \cos(\mathbf{k}'' \cdot \mathbf{q})]$$
$$= \alpha(q)k^2 + \beta(q)k^2 \left(\frac{\mathbf{k} \cdot \mathbf{q}}{kq}\right)^2, \tag{58}$$

and $\lambda(k)$ also reads as

$$\lambda(k) = \int \frac{d\mathbf{q}d\mathbf{k}'}{(2\pi)^3} \frac{(\mathbf{k}' \cdot \mathbf{k})^2}{(k'^2 + \mu^2)k^2} e^{i\mathbf{k}'\cdot\mathbf{q}}(e^{i\mathbf{k}\cdot\mathbf{q}} - 1)$$
$$\times e^{-\alpha(q)k'^2 - \beta(q)k'^2(\mathbf{k}'\cdot\mathbf{q})^2/(k'q)^2}. \tag{59}$$

The computation of the force-velocity power spectrum $P_{\theta\zeta}$ is obtained in the same fashion by considering the correlation $C_{\theta\zeta}(Q)$, where we replace χ in Eq. (43) by θ. As in Eq. (54), this gives

$$P_{\theta\zeta}(k) = P_{\theta\chi}(k)\lambda(k), \tag{60}$$

with the same factor $\lambda(k)$.

Thus, $\lambda(k)$ plays the role of a damping factor, which will lessen the positive correlation between the force and the displacement and velocity fields, as compared with the linear theory where $\lambda_L = 1$.

2. Absence of infrared divergences

We note that λ only depends on the relative displacements, as was expected from the expression (13) of the gravitational force, which only depends on relative distances. This is because we work in a Lagrangian approach and only consider equal-times statistics (associated with the probability distribution $\mathcal{P}$). Then, uniform displacements and velocities have no effect on the divergences $\chi = -\nabla_\mathbf{q} \cdot \mathbf{\Psi}$ and $\theta = -\nabla_\mathbf{q} \cdot \mathbf{v}$. This ensures that spurious infrared divergences or large infrared contributions, which arise in Eulerian approaches and then need special care [57–60], do

not appear at all in our approach. This can be seen in Eq. (55) through the fact that the argument of the last exponential is not the one-point displacement variance, given by

$$\alpha_\infty = \frac{4\pi}{3} \int_0^\infty dk P_{\chi\chi}(k) = \frac{1}{3} \langle |\mathbf{\Psi}(0)|^2 \rangle$$
$$= \lim_{q\to\infty} \frac{1}{6} \langle |\mathbf{\Psi}(\mathbf{q}) - \mathbf{\Psi}(0)|^2 \rangle, \tag{61}$$

such that

$$\int d\mathbf{k}'' P_{\chi\chi}(k'') \frac{(\mathbf{k} \cdot \mathbf{k}'')^2}{k''^4} = \alpha_\infty k^2. \tag{62}$$

In contrast, Eq. (55) depends on the two-point relative displacement variance over Lagrangian distance q, associated with the factor $1 - \cos(\mathbf{k}'' \cdot \mathbf{q})$. This factor damps the contribution of long wavelengths and regularizes the infrared divergences that can appear in Eulerian or different-times approaches.

3. Behavior of the variances $\alpha(q)$ and $\beta(q)$

We shall see below that we obtain a displacement power spectrum $P_{\chi\chi}(k)$ that decays faster than k^{-3} at large k. This implies the small-scale behaviors

$$q \to 0: \quad \alpha = \alpha_0 q^2 + ..., \quad \beta = \beta_0 q^2 + ..., \tag{63}$$

where the dots stand for higher-order terms in q and we have

$$\alpha_0 = \frac{\beta_0}{2} = \frac{2\pi}{15} \int_0^\infty dk k^2 P_{\chi\chi}(k) > 0. \tag{64}$$

At large scales we have

$$q \to \infty: \quad \alpha \to \alpha_\infty, \quad \beta \to 0, \tag{65}$$

provided $P_{\chi\chi}(k)$ increases more slowly than $1/k$ at low k.

4. Behavior of the damping factor $\lambda(k)$

Linear regime.—At early times, the amplitude of the power spectrum $P_{\chi\chi}$ and of the displacement variances α and β vanish. Then, the last exponential in Eq. (59) goes to unity and the integration over $\mathbf{q}$ gives $\lambda = 1$,

$$\alpha \to 0, \quad \beta \to 0: \quad \lambda \to 1. \tag{66}$$

Thus, we recover the linear regime with $P_{\chi\zeta} = P_{\chi\chi}$ and $P_{\theta\zeta} = P_{\theta\chi}$.

Large scales.—The limit of large scales corresponds to $k \to 0$. This is not equivalent to the limit $P_{\chi\chi} \to 0$. For instance, SPT corresponds to expansions over powers of

$P_L(k)$ [10], which corresponds to the limit $P_L \rightarrow 0$, whereas EFT approaches [22,23] consider the limit $k \rightarrow 0$. This can include nonperturbative terms, such as $P_L(k)\frac{k^2}{k_{NL}^2}e^{-1/\sigma^2}$, where k_{NL} is the wave number that marks the transition to the nonlinear regime and σ^2 is a displacement variance such as α and β. These terms do not scale as integer powers of P_L and are beyond the reach of standard perturbative expansions because of the exponential. They arise from shell crossing and the factor e^{-1/σ^2} describes the probability of shell crossing or gravitational collapse for Gaussian initial conditions. (In EFT approaches, the non-perturbative factor is not derived but obtained from fits to numerical simulations and inserted as a coefficient of higher derivative operators in the effective Lagrangian or equations of motion.) Nevertheless, as seen in Appendix A, we recover the linear regime in the large-scale limit

$$k \rightarrow 0: \quad \lambda \rightarrow 1. \qquad (67)$$

This means that, as usual, the linear regime and the large-scale limit coincide at leading order.

Small scales.—As seen in Appendix A, we have the small-scale behavior

$$k \rightarrow \infty: \quad \lambda(k) \sim \lambda_\infty \ln(k), \qquad (68)$$

with

$$\lambda_\infty = -\frac{e^{-1/(12\alpha_0)}}{6\sqrt{3\pi}\alpha_0^{3/2}}. \qquad (69)$$

Thus, in the nonlinear regime, the damping factor λ decreases below unity and actually goes to $-\infty$. This will give rise to a strong deviation of the power spectrum $P_{\chi\chi}(k)$ from the linear power spectrum $P_L(k)$. The nonperturbative reach of our approach appears clearly in Eq. (69) through the nonperturbative exponential factor, which vanishes at all orders of perturbation theory in powers of P_L.

C. Density power spectrum

With the Gaussian *Ansatz* (34), we can compute the density power spectrum (24) exactly as for the Zeldovich approximation [28]. Indeed, although the displacement field $\mathbf{\Psi}(\mathbf{q})$ is no longer given by linear theory, it is still Gaussian within this approximation and the statistical average in Eq. (24) is again straightforward. Using Eq. (50), we obtain for $k > 0$

$$P(k) = \int \frac{d\mathbf{q}}{(2\pi)^3} e^{i\mathbf{k}\cdot\mathbf{q} - \int d\mathbf{k}' P_{\chi\chi}(k')[1-\cos(\mathbf{k}'\cdot\mathbf{q})](\mathbf{k}\cdot\mathbf{k}')^2/k'^4}. \qquad (70)$$

This is the same expression as for the Zeldovich power spectrum, except that the linear power spectrum $P_L(k)$ in the exponent is replaced by the nonlinear power spectrum $P_{\chi\chi}(k)$. With the notations of Eq. (58), this also reads as

$$P(k) = \int \frac{d\mathbf{q}}{(2\pi)^3} e^{ikq\mu - \alpha(q)k^2 - \beta(q)k^2\mu^2}, \qquad (71)$$

where $\mu = (\mathbf{k}\cdot\mathbf{q})/(kq)$ is the cosine of the angle between $\mathbf{k}$ and $\mathbf{q}$. We can integrate over angles to obtain [54,61]

$$P(k) = \int \frac{dq}{2\pi^2} q^2 e^{-(\alpha+\beta)k^2} \sum_{\ell=0}^{\infty} \left(\frac{2\beta k}{q}\right)^\ell j_\ell(kq). \qquad (72)$$

We describe in Appendix B our numerical method to compute the power spectrum (71).

The power spectrum associated with the standard Zeldovich approximation [28] is also given by Eqs. (70) and (71), where we replace the nonlinear power $P_{\chi\chi}$ and variances $\{\alpha, \beta\}$ by their linear values [54,55,61],

$$P_Z(k) = \int \frac{d\mathbf{q}}{(2\pi)^3} e^{ikq\mu - \alpha_L(q)k^2 - \beta_L(q)k^2\mu^2}. \qquad (73)$$

In particular, the same numerical methods can be used for our model (71) and for the Zeldovich power spectrum (73).

V. COMPARISON WITH SOME OTHER APPROACHES

In comparison with previous studies, this work is to some extent a continuation of [62], where we developed a Lagrangian-space *Ansatz* designed to go beyond perturbation theory. That model matched SPT up to one-loop order on large scales and a halo model [63] on small scales, by combining various elements. It included some parameters fitted to numerical simulations (e.g., the halo mass function and the halo profiles) to recover at high k a halo model defined *a priori*. In contrast, in the approach presented in this paper, we do not enforce any specific behavior on either large or small scales and we have no free parameters.

Our method is also related to [37], as it is based on a Lagrangian approach, in order to go beyond shell crossing, and on statistical quantities instead of individual realizations of the fields. However, [37] considered the generating functional $Z[\mathbf{j}]$ of correlation functions, which is then expanded up to some finite order. This means that the equation of motion, which enters the action, is also expanded and approximated up to some order. In addition, [37] introduced by hand an auxiliary truncation of the linear power spectrum, to separate the modes that are kept in the Gaussian part and in the expanded part. In contrast, in this paper we work with the probability distribution functional $\mathcal{P}(\mathbf{\Psi}, \mathbf{v}, t)$ (in practice, it is defined by the power spectra in the Gaussian case) and we do not expand the equations of motion, which are exactly taken into account at the full nonlinear level (but we only include a few of them, among the infinite number of constraints obeyed by the n-point correlations). Also, we do not introduce a truncation of the linear power spectrum of the displacement field. It arises from the equations of motion themselves.

Our work is also related to [46,57], as it is based on the evolution with time of the distribution functional $\mathcal{P}$ of the fields. However, [46] considered the probability distribution $\mathcal{P}(\delta, \theta)$ of the Eulerian density and velocity divergence fields, whereas we consider the probability distribution of the Lagrangian displacement field. Then, they assume a curl-free velocity field, based on the Euler equation, which breaks down beyond shell crossing. They also perform an expansion of the probability distribution $\mathcal{P}(\theta)$, written under the form $e^{-\sum_n \Gamma_n \theta^n}$, by expanding over the non-Gaussian terms $n \geq 3$. In particular, the Gaussian part is given by $\Gamma_2 = 1/P_L(k)$ and the nonlinearity of the gravitational dynamics is captured by the higher orders Γ_n, $n \geq 3$. In a fashion somewhat similar to SPT, these higher-order vertices are obtained from recursion relations that follow from the evolution equation of $\mathcal{P}(\theta)$. The spirit of the approach proposed in this paper is quite different in this respect. Instead of capturing the nonlinearities of the dynamics by adding higher-order terms, such as higher powers in P_L in SPT or higher-order vertices Γ_n, the nonlinearity is already partly taken into account in the Gaussian part of the probability distribution, as the displacement and velocity power spectra get modified from the linear prediction. Following the analogy with the minimization problem of a cost functional $S[\varphi(x)]$, discussed in the Introduction and in Sec. II C, our strategy is not to estimate the minimum $\varphi_{\min}$ by expanding φ around the known minimum φ_0 of a simpler cost functional S_0, in powers of $S - S_0$. Instead, we look for the exact minimum in a simpler subspace of $\{\varphi\}$. For instance, if $\varphi_0(x) = a_0(x - b_0)^2$ is quadratic, the strategy at lowest order is simply to let free the parabola parameters a_0 and b_0 and find their new values $\{a, b\}$ that minimize the new functional S. Clearly, this allows one to reach minima that are very far from the initial guess φ_0 and obtain nonperturbative results. In practice, this means that we avoid explicit perturbative expansions.

Thus, we emphasize that the result (54) and (55) is nonperturbative. Indeed, we do not expand on the displacements Ψ, which are not assumed to be small. Within the Gaussian *Ansatz* for the probability distribution $\mathcal{P}$, we perform the exact computation of the displacement-force correlation $\langle \chi \zeta \rangle$, using the exact expression (13) of the gravitational force. Thus, our approach follows a strategy that is quite different from usual perturbative methods. We do not expand the equations of motion either, which are kept at a fully nonlinear level as in (30)–(32), but we only include the lowest-order ones. Then, the approximation scheme, or truncation, occurs instead at the level of the trial distribution $\mathcal{P}$.

For the simplest Gaussian *Ansatz* considered in this paper, this program is easy to complete, as exact computations are easily performed for Gaussian fields. However, for higher orders, that is, for more complex *Ansätze* that go beyond the Gaussian, this may represent a much more

difficult task. Indeed, to fulfil the nonperturbative promise of this approach, we would need again to compute exactly quantities such as $\langle \Psi F \rangle$. This may prove much more difficult for non-Gaussian probability distributions and represent a drawback of this approach.

In terms of the density field, Eq. (70) coincides with a truncated Zeldovich approximation [64]. However, in our case the truncation is not set *a priori* with a cutoff that follows from an educated guess or a fit to numerical simulation. Instead, the cutoff $\lambda(k)$ is generated by the equations of motion themselves and there are no free parameters to be fitted to simulations. This represents a significant improvement over most previous analytical approaches, which either fail to regularize small-scale divergences (such as SPT) or introduce counterterms with an amplitude that must be measured in simulations (such as EFT methods).

As in EFT methods [22,23], the ultraviolet divergences, or artificially large contributions, associated with the continuous rise of the linear density fluctuations on small scales, are tamed. In EFT this is done by introducing counterterms to the SPT diagrammatic computations, which arise from new operators in the Lagrangian or the equations of motion. The latter are expected to describe the effects of multistreaming that are not included in the hydrodynamical equations of motion. They are obtained from systematic large-scale expansions, but with free coefficients that must be fitted to numerical simulations. In our approach, as we shall see in the next sections, the displacement linear power spectrum is damped at high k by the factor $\lambda(k)$ in Eq. (54). As in the truncated Zeldovich approximation [64], this removes ultraviolet divergences and provides an implicit regularization. For instance, we shall see that in Sec. VI C 1 that, even when the standard Zeldovich power spectrum does not exist, because of such ultraviolet divergences, our approach remains well defined. In contrast with EFT methods, this does not involve free parameters and new operators, and this self-regularization directly follows from the equations of motion.

VI. SELF-SIMILAR DYNAMICS

A. Differential equations for power spectra

To illustrate our approach, we consider in this section the simpler case of the Einstein–de Sitter cosmology, $\Omega_m = 1$, where $D(t) = a(t)$, and the initial linear power spectrum is a power law,

$$P_L(k) \propto k^n. \tag{74}$$

Then, because Newtonian gravity is scale free, it is well known that the dynamics are self-similar [65] and statistics no longer depend on time once they are expressed in units of the nonlinear wave number $k_{\mathrm{NL}}(t)$ that marks the transition to the nonlinear regime. Defining, for instance, $k_{\mathrm{NL}}(\eta)$ by

$$4\pi k_{NL}^3 P_L(k_{NL}, \eta) = 1, \tag{75}$$

the linear power spectrum can be written as

$$P_L(k, \eta) = \frac{e^{2\eta}}{4\pi k_0^3}\left(\frac{k}{k_0}\right)^n = \frac{1}{4\pi k_{NL}^3}\left(\frac{k}{k_{NL}}\right)^n, \tag{76}$$

where k_0 defines the normalization of the linear power spectrum and $k_{NL}(\eta)$ is given by

$$k_{NL}(\eta) = k_0 e^{-2\eta/(n+3)}. \tag{77}$$

Then, all power spectra have the self-similar form

$$P(k, \eta) = \frac{1}{4\pi k^3}\mathcal{D}\left(\frac{k}{k_{NL}(\eta)}\right) = \frac{1}{4\pi k^3}\mathcal{D}\left(\frac{k}{k_0}e^{2\eta/(n+3)}\right), \tag{78}$$

with the scaling function $\mathcal{D}$ that only depends on the ratio k/k_{NL}. In the linear regime, we have $\mathcal{D}_L(x) = x^{n+3}$. The self-similar evolution (78) implies the relation

$$\frac{\partial P}{\partial \eta} = \frac{2}{n+3}\left(k\frac{\partial P}{\partial k} + 3P\right). \tag{79}$$

This exact relation allows us to replace time derivatives of statistical quantities by spatial derivatives. Using also $\Omega/f^2 = 1$ in the Einstein–de Sitter cosmology, Eqs. (30)–(32) simplify as

$$\frac{2}{n+3}\left(\frac{\partial P_{\chi\chi}}{\partial \ln k} + 3P_{\chi\chi}\right) = 2P_{\chi\theta}, \tag{80}$$

$$\frac{2}{n+3}\left(\frac{\partial P_{\chi\theta}}{\partial \ln k} + 3P_{\chi\theta}\right) = P_{\theta\theta} - \frac{1}{2}P_{\chi\theta} + \frac{3}{2}P_{\chi\zeta}, \tag{81}$$

$$\frac{2}{n+3}\left(\frac{\partial P_{\theta\theta}}{\partial \ln k} + 3P_{\theta\theta}\right) = -P_{\theta\theta} + 3P_{\theta\zeta}. \tag{82}$$

Introducing the 3D power $\Delta^2(k, \eta)$ per logarithmic interval of wave number by

$$\Delta^2(k, \eta) = 4\pi k^3 P(k, \eta) = \mathcal{D}\left(\frac{k}{k_{NL}}\right), \tag{83}$$

and the wave number scaling coordinate u,

$$u = (n+3)\ln\left(\frac{k}{k_{NL}}\right), \tag{84}$$

the system (80)–(82) writes

$$\mathcal{D}'_{\chi\chi} = \mathcal{D}_{\chi\theta}, \tag{85}$$

$$\mathcal{D}'_{\chi\theta} = -\frac{1}{4}\mathcal{D}_{\chi\theta} + \frac{1}{2}\mathcal{D}_{\theta\theta} + \frac{3}{4}\mathcal{D}_{\chi\zeta}, \tag{86}$$

$$\mathcal{D}'_{\theta\theta} = -\frac{1}{2}\mathcal{D}_{\theta\theta} + \frac{3}{2}\mathcal{D}_{\theta\zeta}, \tag{87}$$

where the prime denotes the derivative with respect to u. The linear regime corresponds to all $\mathcal{D}_{\star\star}$ identical with

$$\mathcal{D}_L(u) = e^u. \tag{88}$$

Thanks to the self-similarity (78), the system of partial differential equations (30)–(32) has been transformed into a system of ordinary differential equations. These equations are exact but require the force cross-power spectra $P_{\chi\zeta}$ and $P_{\theta\zeta}$ to form a closed system.

B. Curl-free Gaussian *Ansatz*

Within the curl-free Gaussian *Ansatz* presented in Sec. IV, we can close the system (85)–(87) thanks to Eqs. (54) and (60). This gives

$$\mathcal{D}'_{\chi\chi} = \mathcal{D}_{\chi\theta}, \tag{89}$$

$$\mathcal{D}'_{\chi\theta} = \frac{3}{4}\lambda\mathcal{D}_{\chi\chi} - \frac{1}{4}\mathcal{D}_{\chi\theta} + \frac{1}{2}\mathcal{D}_{\theta\theta}, \tag{90}$$

$$\mathcal{D}'_{\theta\theta} = \frac{3}{2}\lambda\mathcal{D}_{\chi\theta} - \frac{1}{2}\mathcal{D}_{\theta\theta}. \tag{91}$$

By combining these three equations, we can eliminate $\mathcal{D}_{\chi\theta}$ and $\mathcal{D}_{\theta\theta}$ to obtain a third-order linear equation over $\mathcal{D}_{\chi\chi}$,

$$\mathcal{D}'''_{\chi\chi} + \frac{3}{4}\mathcal{D}''_{\chi\chi} + \left(\frac{1}{8} - \frac{3\lambda}{2}\right)\mathcal{D}'_{\chi\chi} - \left(\frac{3\lambda}{8} + \frac{3\lambda'}{4}\right)\mathcal{D}_{\chi\chi} = 0. \tag{92}$$

The general solution of this equation is [66]

$$\mathcal{D}_{\chi\chi}(u) = e^{-u/4}[c_1 y_1(u)^2 + c_2 y_1(u)y_2(u) + c_3 y_2(u)^2], \tag{93}$$

where c_i are constants and $y_i(u)$ are two independent solutions of the second-order linear differential equation

$$y'' - \frac{24\lambda + 1}{64}y = 0. \tag{94}$$

On large scales, that is, for large negative u, we have $\lambda = 1$ and the two independent solutions are $y_1 = e^{5u/8}$ and $y_2 = e^{-5u/8}$. The matching to the linear regime (88) implies $c_2 = c_3 = 0$ in Eq. (93). Therefore, we obtain

$$\mathcal{D}_{\chi\chi}(u) = e^{-u/4}y(u)^2 \geq 0, \tag{95}$$

where $y(u)$ is the solution of Eq. (94) with the boundary condition at large negative u

$$u \to -\infty: \quad y(u) = e^{5u/8}. \tag{96}$$

On small scales, that is, for $u \to \infty$, we have from Eq. (68) $\lambda \sim -|\lambda_\infty| u/(n+3)$. This gives the asymptotic behavior

$$u \to \infty: \quad y(u) = c_1 \text{Ai}(-\gamma_\infty u) + c_2 \text{Bi}(-\gamma_\infty u), \quad (97)$$

where $\text{Ai}(x)$ and $\text{Bi}(x)$ are the Airy functions of the first and second kind, c_i are constants and γ_∞ is given by

$$\gamma_\infty = \left(\frac{3|\lambda_\infty|}{8(n+3)} \right)^{1/3}. \quad (98)$$

From the asymptotic behaviors of the Airy functions, we obtain

$$k \gg k_{\text{NL}}: \quad \Delta^2_{\chi\chi}(k,\eta) \sim \left(\frac{k}{k_{\text{NL}}} \right)^{-(n+3)/4}$$
$$\times [\ln(k/k_{\text{NL}})]^{-1/2} [c_1 \sin\psi + c_2 \cos\psi]^2, \quad (99)$$

where c_i are constants and $\psi(k,\eta)$ is given at leading order by

$$\psi(k,\eta) \sim \sqrt{\frac{|\lambda_\infty|}{6}} (n+3) [\ln(k/k_{\text{NL}})]^{3/2}. \quad (100)$$

From Eqs. (89) and (90) and Eq. (95) we obtain for the other power spectra

$$\mathcal{D}_{\chi\theta}(u) = e^{-u/4} \left(-\frac{y^2}{4} + 2yy' \right), \quad (101)$$

$$\mathcal{D}_{\theta\theta}(u) = e^{-u/4} \left(\frac{y}{4} - 2y' \right)^2 \geq 0. \quad (102)$$

Omitting the sine and cosine factors, this gives the small-scale behaviors

$$k \gg k_{\text{NL}}: \Delta^2_{\chi\theta}(k,\eta) \sim \left(\frac{k}{k_{\text{NL}}} \right)^{-(n+3)/4}, \quad (103)$$

$$\Delta^2_{\theta\theta}(k,\eta) \sim \left(\frac{k}{k_{\text{NL}}} \right)^{-(n+3)/4} [\ln(k/k_{\text{NL}})]^{1/2}. \quad (104)$$

Thus, at leading order the three logarithmic power spectra decay as $\Delta^2_{**}(k) \propto k^{-(n+3)/4}$, and the power spectra decays faster than k^{-3}, as $P_{**}(k) \propto k^{-3-(n+3)/4}$. This leads to the universal behavior (63), independent of the exponent n of the linear power spectrum.

A remarkable feature of the solutions (95), (103), and (104) is that the autopower spectra $\Delta^2_{\chi\chi}$ and $\Delta^2_{\theta\theta}$ are always positive, whereas the cross-power spectrum $\Delta^2_{\chi\theta}$ can change sign. By definition, autopower spectra must be positive, but this property is often violated in approximation schemes, such as perturbative expansions. Indeed, terms of successive orders can become increasingly large with alternating

signs on nonlinear scales, and the sign of the prediction depends on the truncation order if the series has not converged yet.

In our approach, even though we performed the simplest Gaussian approximation in Sec. IV, the autopower spectra $\Delta^2_{\chi\chi}$ and $\Delta^2_{\theta\theta}$ are always positive. This was not obvious from the differential system (80)–(82) and was not explicitly enforced by additional constraints. This could signal the robustness of our approach. It may follow from the fact that we keep track of the exact equations of motion (80)–(82), and that the cross-power spectra $P_{\chi\zeta}$ and $P_{\theta\zeta}$ are exactly computed from an *Ansatz* that is always physical, albeit different from the true particle distribution (we did not obtain the exact solution of the gravitational dynamics). Indeed, the Gaussian *Ansatz* of Sec. IV corresponds to a physical distribution of particles and velocities so that force cross-power spectra derived in this manner do not hide any inconsistencies. (This is not the case for approaches that start directly at the level of the correlation functions, where it is not always known whether there exists a distribution of particles that provides a physical realization of the *Ansatz* used for the density correlations. Then, this *Ansatz* may contain some inconsistencies, that may be harmful or not, depending on the quantities and regimes of interest.) However, even though we have a physical *Ansatz* at each time, we do not follow the exact dynamics. Therefore, there is no guarantee that our integration of (80)–(82) avoids all inconsistencies. Nevertheless, this approach is clearly a step in the direction toward self-consistency and it appears to be sufficient to ensure positivity of displacement and velocity autopower spectra.

C. Numerical computation

To obtain the power spectra $\mathcal{D}_{**}(u)$, we need to solve the differential equation (94), where $\lambda(u)$ depends on $\mathcal{D}_{\chi\chi}(u)$ through Eq. (59). This gives a nonlinear system of equations, which we solve by an iterative procedure. Starting with an initial guess for $\mathcal{D}_{\chi\chi}(u)$, which converges to the linear regime (88) for $u \ll -1$ and decays as $e^{-u/4}$ for $u \gg 1$, we compute from Eq. (59) the damping factor $\lambda(u)$. The expressions that we use in practice for the numerical computations are given in Appendix A. Then, we obtain $y(u)$ from Eq. (94), and the power spectra from (95), (101), and (102). Next, we repeat the procedure, computing λ, y, and $\mathcal{D}_{**}$ from this new power spectrum $\mathcal{D}_{\chi\chi}$. We iterate until the damping factor λ and the power spectra have converged. Finally, from the displacement power spectrum $P_{\chi\chi}$ we obtain the density power spectrum $P(k)$ from Eq. (70). Our numerical procedure is described in Appendix B.

We normalize the linear power spectra by $k_{\text{NL}} = 1$,

$$k_{\text{NL}} = 1: \quad P_L(k) = \frac{k^n}{4\pi}. \quad (105)$$

This also means that the Lagrangian scale q_{NL} that marks the transition to the nonlinear regime is of order unity. We

have noticed in Sec. IV B 3 that the variances $\{\alpha, \beta\}$ show the universal behavior (63) at small q, because the non-linear power spectrum $P_{\chi\chi}(k)$ decays faster than k^{-3} from Eq. (99). At large separation q, the displacement variances (56) and (57) are governed by the low-k part of the power spectrum $P_{\chi\chi}(k)$, which converges to the linear power spectrum $P_L(k)$. This gives

$$q \gg q_{\mathrm{NL}}: \quad \beta(q) \propto q^{-(n+1)} \quad \text{for } -3 < n < 1, \quad (106)$$

and

$$\alpha(q) \propto q^{-(n+1)} \rightarrow \infty \quad \text{for } -3 < n < -1,$$
$$\alpha(q) \rightarrow \alpha_\infty \quad \text{for } -1 < n < 1. \quad (107)$$

1. Self-similar case with n = 0

We first consider for illustration the case $n = 0$. We show in Fig. 1 the variances $\alpha(q)$ and $\beta(q)$ defined by the final nonlinear power spectrum $P_{\chi\chi}(k)$, once the iterative procedure explained above has converged. We recover the small-scale quadratic behavior (63) and the large-scale behavior (106) and (107), with a transition at $q_{\mathrm{NL}} \sim 1$.

We display in Fig. 2 the damping factor $\lambda(k)$ of Eq. (59). For the numerical computation, we use the expressions given in Appendix A. In agreement with Eqs. (67) and (68), at low k it goes to unity, while at high k it goes to $-\infty$ as $-\ln(k)$. The transition occurs around $k_{\mathrm{NL}} = 1$.

We show in Fig. 3 the displacement and velocity logarithmic power spectra $\Delta_{\chi\chi}^2$, $\Delta_{\chi\theta}^2$, and $\Delta_{\theta\theta}^2$ from Eqs. (95), (101), and (102). At low k, all power spectra converge to the linear power spectrum $\Delta_L^2(k) = k^3$ for the normalization (105). The cross-power spectrum $\Delta_{\chi\theta}^2$ changes sign and we show its absolute value. The power spectra $\Delta_{\chi\chi}^2$ and $\Delta_{\theta\theta}^2$ are always positive, despite their spikes to small but nonzero values. This means that, in the oscillating factor, as in Eq. (99), one of the coefficients c_i is significantly greater than the other, so that $\Delta_{\chi\chi}^2$ almost reaches zero as $\sin^2 \psi$ or $\cos^2 \psi$. Thus, within decaying envelopes, $y(u)$ oscillates as $\cos(\psi - \psi_0)$, where ψ_0 is a constant and ψ was defined in Eq. (104), while $y'(u)$ oscillates in quadrature as $\sin(\psi - \psi_0)$. This implies that, within decaying envelopes, $\Delta_{\chi\chi}^2 \propto y^2 \propto \cos^2(\psi - \psi_0)$ and $\Delta_{\theta\theta}^2 \propto y'^2 \propto \sin^2(\psi - \psi_0)$ oscillate in quadrature. Since $y' \gg y$, we have $\Delta_{\chi\theta}^2 \propto yy'$ and it oscillates twice as fast as $\sin(\psi - \psi_0)$. We can check these phase differences in Fig. 3. The envelope of these power spectra decays as $k^{-3/4}$ at high k, in agreement with Eqs. (99), (103), and (104).

We show in Fig. 4 the nonlinear density power spectrum Δ^2 from Eq. (71), as well as the linear power spectrum $\Delta_L^2 = k^3$. Our numerical computation is described in Appendix B 1. Note that this case $n = 0$ corresponds to a linear power spectrum with a lot of power on small scales.
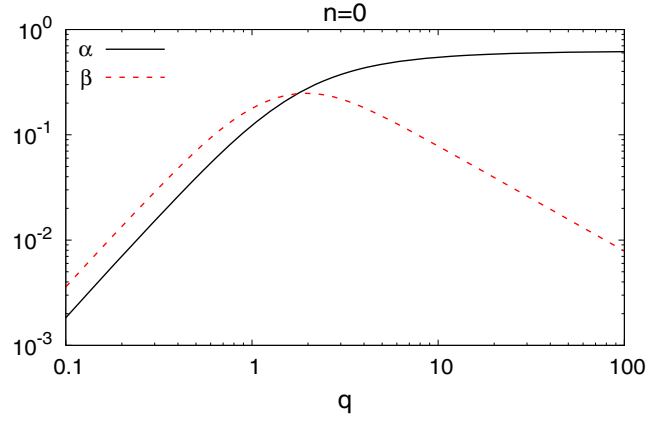

FIG. 1. Variances $\alpha(q)$ and $\beta(q)$ defined by the nonlinear power spectrum $P_{\chi\chi}(k)$ in the power-law case $n = 0$.
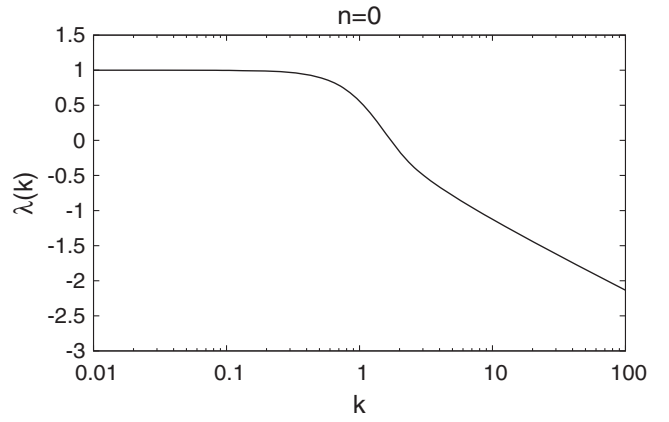

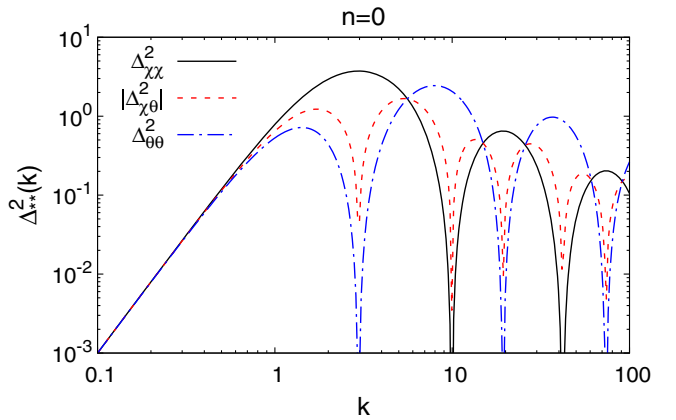FIG. 2. Damping factor $\lambda(k)$ for the power-law case $n = 0$.

FIG. 3. Displacement and velocity logarithmic power spectra $\Delta_{\chi\chi}^2$, $|\Delta_{\chi\theta}^2|$, and $\Delta_{\theta\theta}^2$ for the initial power-law case $n = 0$.

Then, the linear variance $\alpha_L(q)$ defined by Eq. (56) where we replace $P_{\chi\chi}(k)$ by $P_L(k)$ is infinite. This implies that the Zeldovich power spectrum (73) does not exist. Indeed, the standard Zeldovich approximation does not modify
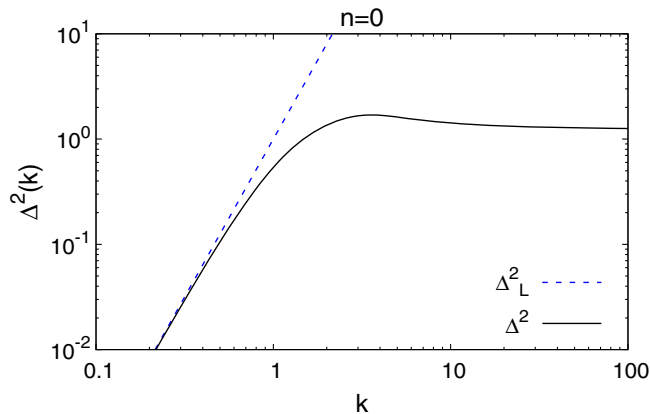
FIG. 4. Density logarithmic power spectrum $\Delta^2(k)$. We show the linear power Δ_L^2 (dashed line) and the nonlinear power Δ^2 (solid line).

the linear displacement field and does not cure small-scale divergences that are already present in the linear theory. More generally, the Zeldovich power spectrum (73) only exists for $-3 < n < -1$ [55,61], where there is no small-scale divergence. This is often cured by using a truncated Zeldovich approximation [64], where the initial linear power spectrum is truncated beyond k_{NL} so that $\alpha_L(q)$ is finite and one can compute a Zeldovich power spectrum (73). This requires introducing an *ad hoc* cutoff parameter, which may be fitted to numerical simulations.

Our approach leads to a density power spectrum that coincides with such a truncated Zeldovich approximation, but the cutoff is not introduced by hand. It is obtained from the equations of motion, as explained in the previous sections, through the computation of the damping factor $\lambda(k)$ and its impact on the nonlinear displacement power spectrum $P_{\chi\chi}$. Another difference from the truncated Zeldovich approximation is that we obtain different results for the velocity power spectra $P_{\chi\theta}$ and $P_{\theta\theta}$.

As for the truncated Zeldovich approximations with a strong enough cutoff, the logarithmic density power spectrum $\Delta^2(k)$ shows a constant asymptote at high k, of order unity. This is because $\Delta_{\chi\chi}^2$ decreases at high k, as found in Eq. (99). This avoids that spurious power on nonlinear scales for the displacement field completely erases small-scale structures and the density power spectrum, as found in the standard (nontruncated) Zeldovich approximation, where $\Delta_Z^2(k)$ typically decreases at high k. For this case $n = 0$ we note, however, that the nonlinear density power spectrum is below the linear power spectrum on mildly nonlinear scales. This is due to the saturation at $\Delta^2 \sim 1$ in the nonlinear regime, whereas the linear power spectrum $\Delta_L^2 \propto k^3$ shows a very steep rise with k for these initial conditions that show a lot of power on small scales. This agrees with the fact that the damping factor $\lambda(k)$ shown in Fig. 2 is everywhere below unity.

Thus, our approach provides a significant improvement over the standard Zeldovich approximation. This suggests

that the general spirit of our method goes in the right direction: letting the power spectra of the displacement and velocity fields free, instead of setting them equal to the linear power spectrum, and obtaining their values from constraints derived from the equations of motion gives a better description of the system. However, our Gaussian *Ansatz* cannot give the continuing increase of $\Delta^2(k)$ on nonlinear scales, typically associated with the "1-halo" term in halo models [62,63] and the formation of high-density virialized halos. It is likely that this would require going beyond the Gaussian and taking into account higher-order correlations (at least three-point correlations).

2. Self-similar case with n = −2

In the case $n = -2$, the initial density and displacement fields show a lot of power on large scales. Then, the variance of the linear displacement difference over separation q grows linearly with q, in agreement with Eqs. (106) and (107). With the normalization (105), we obtain

$$\alpha_L(q) = \beta_L(q) = \frac{\pi}{16} q, \qquad (108)$$

while $\alpha_{L\infty}$ is infinite. This infrared divergence also applies to the nonlinear displacement field, whose power spectrum converges to the linear power spectrum at low k. Thus, we have

$$q \gg q_{NL}: \quad \alpha(q) = \frac{\pi}{16} q + ..., \quad \beta(q) = \frac{\pi}{16} q + ..., \quad (109)$$

where the dots stand for subleading terms, and $\alpha_\infty = +\infty$. We can check the asymptotic behaviors (63) and (109) in Fig. 5.

The damping factor $\lambda(k)$ again goes to unity at low k and to $-\infty$ as $-\ln(k)$ at high k, as seen in Fig. 6. The comparison with Fig. 2 shows that the amplitude of $\lambda(k)$ at fixed wave number k is greater for $n = -2$ than for $n = 0$, in the nonlinear regime. Nevertheless, the decay and
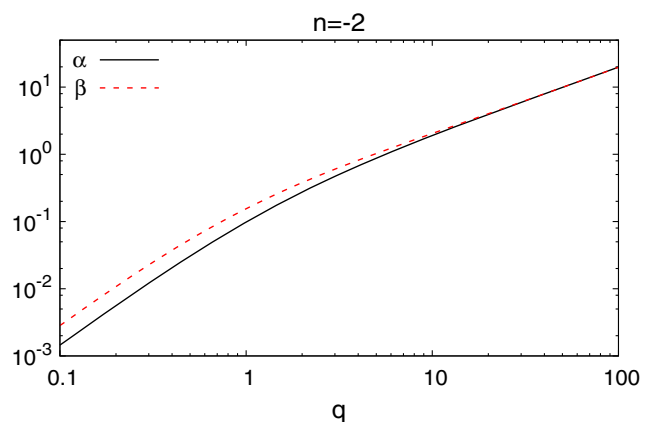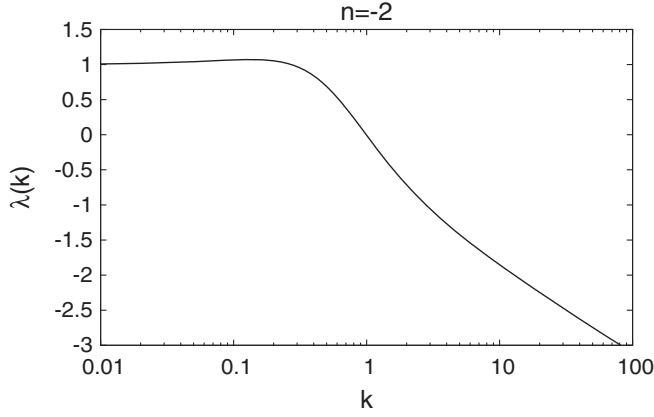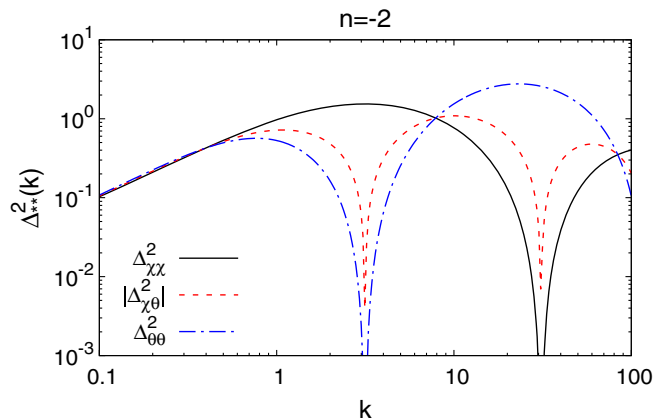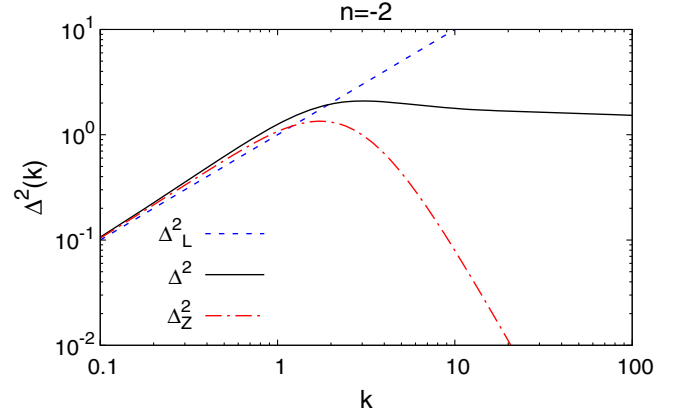

FIG. 5. Variances $\alpha(q)$ and $\beta(q)$ defined by the nonlinear power spectrum $P_{\chi\chi}(k)$ in the power-law case $n = -2$.

FIG. 6. Damping factor $\lambda(k)$ for the power-law case $n = -2$.

FIG. 8. Density logarithmic power spectrum $\Delta^2(k)$. We show the linear power spectrum Δ_L^2 (dashed line), our nonlinear power spectrum Δ^2 (solid line), and the Zeldovich power spectrum Δ_Z^2 (dot-dashed line).

the oscillation rate of the displacement and velocity power spectra $\Delta_{\chi\chi}^2$, $\Delta_{\chi\theta}^2$, and $\Delta_{\theta\theta}^2$ are slower than for the case $n = 0$ in terms of wave number, as seen in Fig. 7. This agrees with the fact that these logarithmic power spectra now decrease as $k^{-1/4}$ instead of $k^{-3/4}$, as shown by Eqs. (99), (103), and (104). We can also see that $\lambda(k)$ now grows slightly above unity at $k \sim 0.2$ before its decreases in the highly nonlinear regime. This means that, in contrast to the case $n = 0$, there is now a small amplification of structure formation as compared with the linear theory on the weakly nonlinear scale $k \sim 0.2$.

We show in Fig. 8 the nonlinear density power spectrum Δ^2 from Eq. (71), as well as the linear prediction Δ_L^2 and the Zeldovich power spectrum Δ_Z^2. Indeed, because the linear variances $\alpha_L(q)$ and $\beta_L(q)$ are now finite, the standard Zeldovich power spectrum (without truncation) exists. In fact, for this power-law case $n = -2$, it is possible to compute analytically the Zeldovich power spectrum (73). For the normalization (105), this gives [61]

$$P_Z(k) = \frac{256}{\pi k^2} \left\{ \frac{4}{(64 + \pi^2 k^2)^2} + \frac{3\pi k(\sqrt{64 + \pi^2 k^2} - 8)}{(64 + \pi^2 k^2)^{5/2}} \right.$$
$$\times \frac{\text{ArcTan}(\pi k/\sqrt{128 + \pi^2 k^2 - 16\sqrt{64 + \pi^2 k^2}})}{\sqrt{128 + \pi^2 k^2 - 16\sqrt{64 + \pi^2 k^2}}}$$
$$+ \frac{3\pi k(\sqrt{64 + \pi^2 k^2} + 8)}{(64 + \pi^2 k^2)^{5/2}}$$
$$\left. \times \frac{\text{ArcTan}(\pi k/\sqrt{128 + \pi^2 k^2 + 16\sqrt{64 + \pi^2 k^2}})}{\sqrt{128 + \pi^2 k^2 + 16\sqrt{64 + \pi^2 k^2}}} \right\},$$

(110)

with the asymptotic behaviors

$$k \to 0: \quad P_Z(k) = \frac{1}{4\pi k^2} + \frac{3\pi}{256 k} + \dots, \quad (111)$$

$$k \to \infty: \quad P_Z(k) = \frac{128(8 + 3\pi)}{\pi^5 k^6} - \frac{4096(32 + 15\pi)}{\pi^7 k^8} + \dots$$

(112)

We describe in Appendix B 2 our numerical computation of the nonlinear density power spectrum (71). Again, we recover the universal plateau at high k of the nonlinear logarithmic power spectrum Δ^2, due to the decay of the displacement logarithmic power spectrum $\Delta_{\chi\chi}^2$ within our Gaussian *Ansatz*. In contrast, the nontruncated Zeldovich power spectrum decays as $\Delta_Z^2(k) \propto k^{-3}$, because of the artificially large power on small scales in the linear displacement field. Thus, our approach improves over the nontruncated Zeldovich approximation. It also improves over the truncated Zeldovich approximation, as there is no need to introduce an *ad hoc* truncation with free parameters. In agreement with the slight increase above unity of the damping factor $\lambda(k)$ at $k \sim 0.2$, and in contrast

FIG. 7. Displacement and velocity logarithmic power spectra $\Delta_{\chi\chi}^2$, $|\Delta_{\chi\theta}^2|$, and $\Delta_{\theta\theta}^2$ for the initial power-law case $n = -2$.

with the case $n = 0$, we now find that the nonlinear power spectrum Δ^2 rises above the linear prediction on weakly nonlinear scales, $k \lesssim 1$. This feature is also seen in the standard Zeldovich approximation (111). This is slightly more apparent in the case of our nonlinear power spectrum Δ^2 because it asymptotes to a constant value at high k instead of decreasing as k^{-3}. The comparison with the case $n = 0$ shows that such detailed features depend on the shape of the initial linear power spectrum. This is consistent with the fact that, within SPT, the one-loop correction to the density power spectrum is positive for $n \lesssim -1.4$ and negative for $n \gtrsim -1.4$ [67–69].

VII. Λ-CDM COSMOLOGY

A. Integration of the curl-free Gaussian *Ansatz*

We now consider the realistic case of the Λ-CDM cosmology with a linear CDM power spectrum that is not a power law. Then, we must go back to the system of partial differential equations (30)–(32). With the curl-free Gaussian *Ansatz* presented in Sec. IV, this reads

$$\frac{\partial \Delta_{\chi\chi}^2}{\partial \eta} = 2\Delta_{\chi\theta}^2, \tag{113}$$

$$\frac{\partial \Delta_{\chi\theta}^2}{\partial \eta} = \frac{3\Omega_m}{2f^2} \lambda \Delta_{\chi\chi}^2 + \left(1 - \frac{3\Omega_m}{2f^2}\right)\Delta_{\chi\theta}^2 + \Delta_{\theta\theta}^2, \tag{114}$$

$$\frac{\partial \Delta_{\theta\theta}^2}{\partial \eta} = \frac{3\Omega_m}{f^2} \lambda \Delta_{\chi\theta}^2 + \left(2 - \frac{3\Omega_m}{f^2}\right)\Delta_{\theta\theta}^2, \tag{115}$$

where we introduced the logarithmic power $\Delta^2(k, \eta)$ as in (83). For the self-similar cases studied in Sec. VI, we reduced the problem to the set of one-dimensional scaling functions $\mathcal{D}_{**}(u)$ and we could solve the associated system of ordinary differential equations. In the general case (113)–(115), thanks to the factorizations (54) and (60), we again obtain a system of ordinary differential equations. Indeed, different wave numbers k decouple, once we consider $\lambda(k, \eta)$ as an external control function, and we can now solve over the time η at fixed k. We can again eliminate $\Delta_{\chi\theta}^2$ and $\Delta_{\theta\theta}^2$ to obtain the third-order linear equation

$$\frac{\partial^3 \Delta_{\chi\chi}^2}{\partial \eta^3} + \left(\frac{9\Omega_m}{2f^2} - 3\right)\frac{\partial^2 \Delta_{\chi\chi}^2}{\partial \eta^2} + \left[2 + \frac{\partial}{\partial \eta}\left(\frac{3\Omega_m}{2f^2}\right)\right.$$
$$\left. - \frac{6\Omega_m}{f^2}(1 + \lambda) + \frac{9\Omega_m^2}{2f^4}\right]\frac{\partial \Delta_{\chi\chi}^2}{\partial \eta} + \left[-\frac{\partial}{\partial \eta}\left(\frac{3\Omega_m}{f^2}\lambda\right)\right.$$
$$\left. + \frac{6\Omega_m}{f^2}\lambda - \frac{9\Omega_m^2}{f^4}\lambda\right]\Delta_{\chi\chi}^2 = 0. \tag{116}$$

Again, the general solution of this ordinary differential equation over η, at fixed k, is [66]

$$\Delta_{\chi\chi}^2(k, \eta) = c_1 y_1(\eta)^2 + c_2 y_1(\eta) y_2(\eta) + c_3 y_2(\eta)^2, \tag{117}$$

where c_i are integration constants that depend on k, and $y_i(\eta)$ are two independent solutions of the second-order linear differential equation

$$y'' + \left(\frac{3\Omega_m}{2f^2} - 1\right)y' - \frac{3\Omega_m}{2f^2}\lambda y = 0, \tag{118}$$

where the prime denotes the derivative with respect to η. Because $\lambda(k, \eta)$ depends on both k and η, the functions $y_i(\eta)$ also depend on k, understood here as a parameter. At early times, in the matter-dominated era, we must recover the linear regime,

$$\eta \to -\infty: \quad \Delta_L^2(k, \eta) = e^{2\eta}\Delta_{L0}^2(k). \tag{119}$$

In this regime, we also have $\Omega_m/f^2 \to 1$ and $\lambda \to 1$, which gives the two solutions $y_1 \propto e^\eta$ and $y_2 \propto e^{-3\eta/2}$. Therefore, the matching to the linear regime at early times gives $c_2 = c_3 = 0$ and we obtain

$$\Delta_{\chi\chi}^2(k, \eta) = y(\eta)^2 \Delta_{L0}^2(k) \geq 0, \tag{120}$$

where $y(\eta)$ is the solution of Eq. (118) with the boundary condition at large negative η,

$$\eta \to -\infty: \quad y(\eta) = e^\eta. \tag{121}$$

This gives for the other power spectra

$$\Delta_{\chi\theta}^2(k, \eta) = yy'\Delta_{L0}^2(k), \quad \Delta_{\theta\theta}^2(k, \eta) = y'^2\Delta_{L0}^2(k) \geq 0. \tag{122}$$

Over a limited range of wave numbers and times, the dynamics can be approximated by a self-similar evolution with an effective index n. Then, from Eq. (77) and $\lambda \sim -|\lambda_\infty|\ln(k/k_{\mathrm{NL}})$ we obtain $\lambda \sim -|\lambda_\infty|2\eta/(n+3)$. This gives $y(\eta) \sim e^{-\eta/4}[\mathrm{Ai}(-\eta) + \mathrm{Bi}(-\eta)]$, where we omit numerical factors in the bracket and in the argument of the Airy functions. This gives

$$\eta \gg \eta_{\mathrm{NL}}: \quad \Delta_{\chi\chi}^2(k, \eta) \sim e^{-\eta/2}[\mathrm{Ai}(-\eta) + \mathrm{Bi}(-\eta)]^2, \tag{123}$$

where $\eta_{\mathrm{NL}}(k)$ is the time that marks the entry of the wave number k into the nonlinear regime. At leading order, this gives for all logarithmic power spectra

$$\eta \gg \eta_{\mathrm{NL}}: \quad \Delta_{**}^2(k, \eta) \sim e^{-\eta/2}, \tag{124}$$

which agrees with Eqs. (99), (103), and (104), using Eq. (77). Since this nonlinear decay with time does not depend on the index n, it should be quite robust and a good approximation for the Λ-CDM cosmology, with a smooth initial power spectrum. In a similar fashion, the power spectra should decay with wave number as

$$k \gg k_{\mathrm{NL}}: \quad \Delta^2_{**}(k, \eta) \sim k^{-(n+3)/4}, \qquad (125)$$

where n is the local effective exponent of the linear power spectrum.

Remarkably, Eqs. (120) and (122) show that the positivity of the autopower spectra $\Delta^2_{\chi\chi}$ and $\Delta^2_{\theta\theta}$ is still ensured in the general case for any cosmology and initial power spectrum. As noticed in Sec. IV, such positivity constraints are not respected in most perturbative schemes or approximation methods. This is related to the nonperturbative character of our approach, which does not truncate the equations of motion. Moreover, the approximation needed to close our system, entering at the level of the force cross-power spectra, is computed in an exact manner from a physical Gaussian *Ansatz*. That is, although the Gaussian distribution of particles is only an approximate *Ansatz*, the force cross-power spectra associated with this distribution are exactly computed and as such satisfy all physical requirements associated with the constraint that they can be derived from a physical state (e.g., with positive matter density, conservation of matter, etc.).

In fact, the solutions (120) and (122) do not directly rely on the Gaussian *Ansatz*, but on the equality of the damping factors associated with the cross-power spectra of both the displacement and the velocity with the force. Thus, defining $\lambda_{\chi\zeta}(k, \eta)$ and $\lambda_{\theta\zeta}(k, \eta)$ by the ratios

$$\lambda_{\chi\zeta}(k, \eta) \equiv \frac{P_{\chi\zeta}}{P_{\chi\chi}}, \qquad \lambda_{\theta\zeta}(k, \eta) \equiv \frac{P_{\theta\zeta}}{P_{\theta\chi}}, \qquad (126)$$

the solutions (120) and (122) hold as long as $\lambda_{\chi\zeta} = \lambda_{\theta\zeta}$, and we denote λ their common value. This equality may remain a good approximation beyond the Gaussian *Ansatz* and we have seen that it ensures the positivity of the autopower spectra $\Delta^2_{\chi\chi}$ and $\Delta^2_{\theta\theta}$. However, for the exact non-Gaussian dynamics, we generically expect $\lambda_{\chi\zeta}$ and $\lambda_{\theta\zeta}$ to differ in the nonlinear regime. Unfortunately, we could not find an explicit solution of the system (113)–(115) when $\lambda_{\chi\zeta} \neq \lambda_{\theta\zeta}$. In that case, the requirements $\Delta^2_{\chi\chi} \geq 0$ and $\Delta^2_{\theta\theta} \geq 0$ may provide some constraints on the pair $\{\lambda_{\chi\zeta}, \lambda_{\theta\zeta}\}$. However, it is not obvious whether this can be written in a simple explicit form.

B. Numerical computation

As for the self-similar case studied in Sec. VI C, we compute the solution of Eqs. (113)–(115) by an iterative scheme. We start with an initial guess for the power spectrum $\Delta^2_{\chi\chi}(k, \eta)$, which is equal to the linear power spectrum in the linear regime where $\Delta^2_L \leq 1$, and decays, for instance, as $1/k$ at higher wave numbers. This is stored as an initial guess on a 2D grid in $\{k, \eta\}$. Then, we compute the variances $\alpha(q, \eta)$ and $\beta(q, \eta)$ from Eqs. (56) and (57). This gives the damping factor $\lambda(k, \eta)$ from Eq. (59), using again the numerical method described in Appendix A.
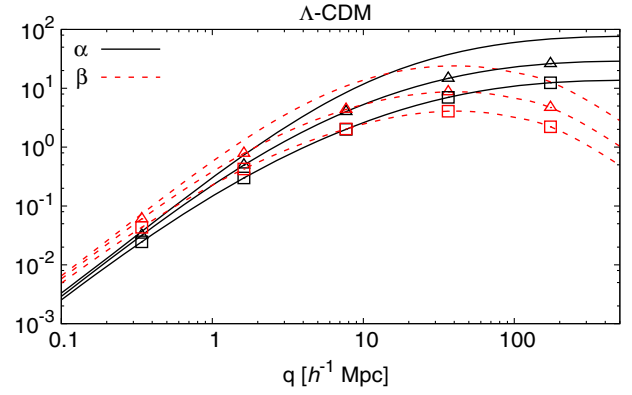

FIG. 9. Variances $\alpha(q)$ and $\beta(q)$ defined by the nonlinear power spectrum $P_{\chi\chi}(k)$ for the Λ-CDM cosmology. We show the results at redshifts $z = 0$ (lines without symbols), $z = 1$ (triangles), and $z = 2$ (squares).

Next, we compute the functions $y(\eta)$, for all grid points k, from Eq. (118). This provides the updated nonlinear displacement and velocity power spectra $\Delta^2_{\chi\chi}$, $\Delta^2_{\chi\theta}$, and $\Delta^2_{\theta\theta}$ through Eqs. (120) and (122). Next, we repeat the procedure, computing $\{\alpha, \beta, \lambda\}$ from the new $\Delta^2_{\chi\chi}$ and next the new spectra Δ^2_{**}. We iterate until convergence. Finally, from the displacement power spectrum $P_{\chi\chi}$ we obtain the density power spectrum $P(k)$ from Eq. (70), using again the numerical method described in Appendix B 1. We do not make the approximation $\Omega/f^2 \simeq 1$ that is often used in analytical studies and we exactly integrate Eq. (118) over time.

We show the variances $\alpha(q)$ and $\beta(q)$ at redshifts $z = 0$, 1, and 2 in Fig. 9. Again, we have the quadratic behavior (63) on small scales. At large distances, the displacement variances are governed by the low-k part of the displacement power spectrum, which converges to the linear power spectrum with $P_L(k) \propto k^n$ and $n \simeq 0.96$ for the Λ-CDM cosmology. In this respect, we are in the same class of initial conditions as for the self-similar case with $n = 0$; $\alpha(q)$ goes to a finite value α_∞, whereas $\beta(q)$ decreases as $q^{-(n+1)}$, as in Eqs. (106) and (107). The small change in the shape of the functions $\alpha(q)$ and $\beta(q)$ with redshift is due to the fact that the Λ-CDM linear power spectrum is curved, with the local slope ranging from $n \simeq 0.96$ at low k to $n \simeq -3$ at high k. In particular, the infinite-separation variance α_∞ of Eq. (61) is governed by the scale k_{-1}, where the local exponent is $n = -1$. This is significantly larger than the scale k_{NL} associated with the nonlinear transition of the matter density power spectrum. Thus, in contrast with the self-similar case $n = 0$, α_∞ can be significantly greater than $1/k^2_{\mathrm{NL}}$, especially at high z. In contrast with some Eulerian-space perturbative schemes, this is not a problem for our approach as it only depends on relative displacements, as seen in Eq. (70), and it is independent of the value of α_∞. This is clear from the fact that our approach can also
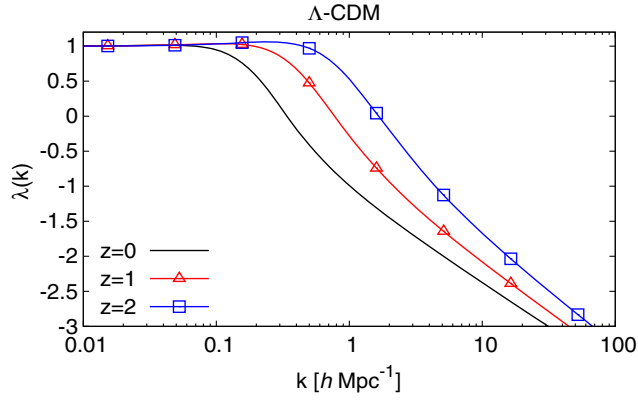
FIG. 10. Damping factor $\lambda(k)$ for the Λ-CDM cosmology, at redshifts $z = 0$ (lines without symbols), $z = 1$ (triangles), and $z = 2$ (squares).

be applied to the self-similar case $n = -2$, where α_∞ is infinite (see Sec. VI C 2 and Appendix B 2).

We display in Fig. 10 the damping factor $\lambda(k)$ at redshifts $z = 0$, 1, and 2. Again, it goes to unity at low k and to $-\infty$ as $-\ln(k)$ at high k. At high redshift $z = 2$, where the effective exponent on weakly nonlinear scales is $n \simeq -2$, we distinguish a small excursion above unity for $\lambda(k)$
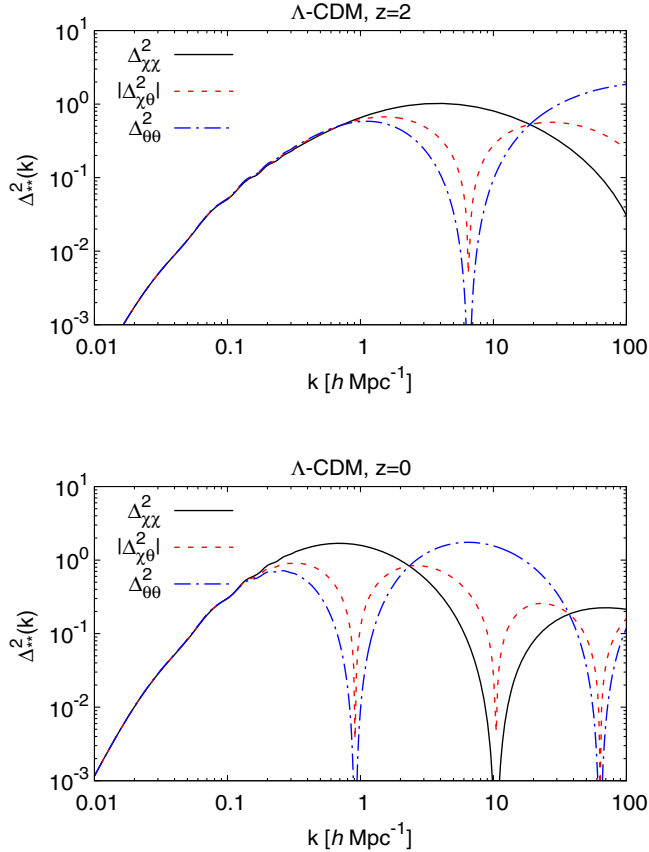
around $k \sim 0.3h$ Mpc^{-1}, in agreement with the self-similar case $n = -2$ shown in Fig. 6. At low redshift $z = 0$, where $n \simeq -1.5$, $\lambda(k)$ remains below unity. This agrees with the behavior found for the self-similar case $n = 0$ shown in Fig. 2.

We show the displacement and velocity power spectra in Fig. 11. In agreement with the analysis in Sec. VII A, on nonlinear scales the power spectra $\Delta^2_{\chi\chi}$ and $\Delta^2_{\theta\theta}$ oscillate in quadrature, whereas $\Delta^2_{\chi\theta}$ oscillates twice faster. Their envelope decays as $\sim k^{-(n+3)/4}$. Again, the evolution with redshift can be understood from the change of the effective exponent n at the scales that are turning nonlinear. At high redshift $z = 2$, where $n \simeq -2$, we recover a slow decay with a large oscillation period over wave number, while at low redshift $z = 0$, where $n \simeq -1.5$, we obtain a stronger decay and faster oscillations. This agrees with Eqs. (99) and (100) and with the comparison of Figs. 3 and 7.

We compare in Fig. 12 the nonlinear matter density power spectrum Δ^2 with the linear prediction Δ^2_L and the Zeldovich power spectrum Δ^2_Z. Again, we find that Δ^2 roughly follows Δ^2_Z on weakly nonlinear scales and next asymptotes to a constant $\Delta^2 \sim 1$ at high k, whereas Δ^2_Z

FIG. 11. Displacement and velocity logarithmic power spectra $\Delta^2_{\chi\chi}$, $|\Delta^2_{\chi\theta}|$, and $\Delta^2_{\theta\theta}$ for the Λ-CDM cosmology.
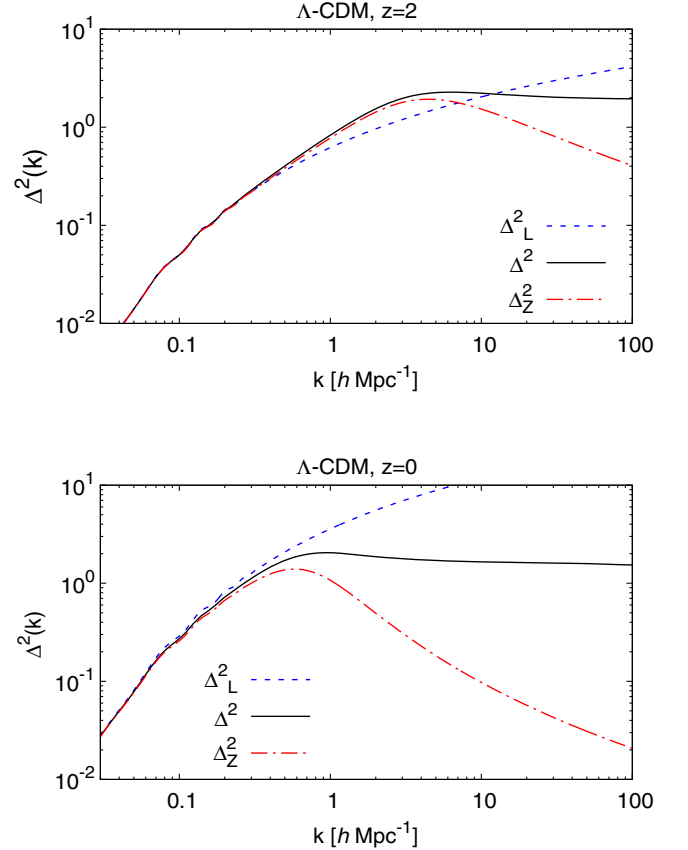

FIG. 12. Density logarithmic power spectrum $\Delta^2(k)$ for the Λ-CDM cosmology. We show the linear power spectrum Δ^2_L (dashed line), our nonlinear power spectrum Δ^2 (solid line), and the Zeldovich power spectrum Δ^2_Z (dot-dashed line).
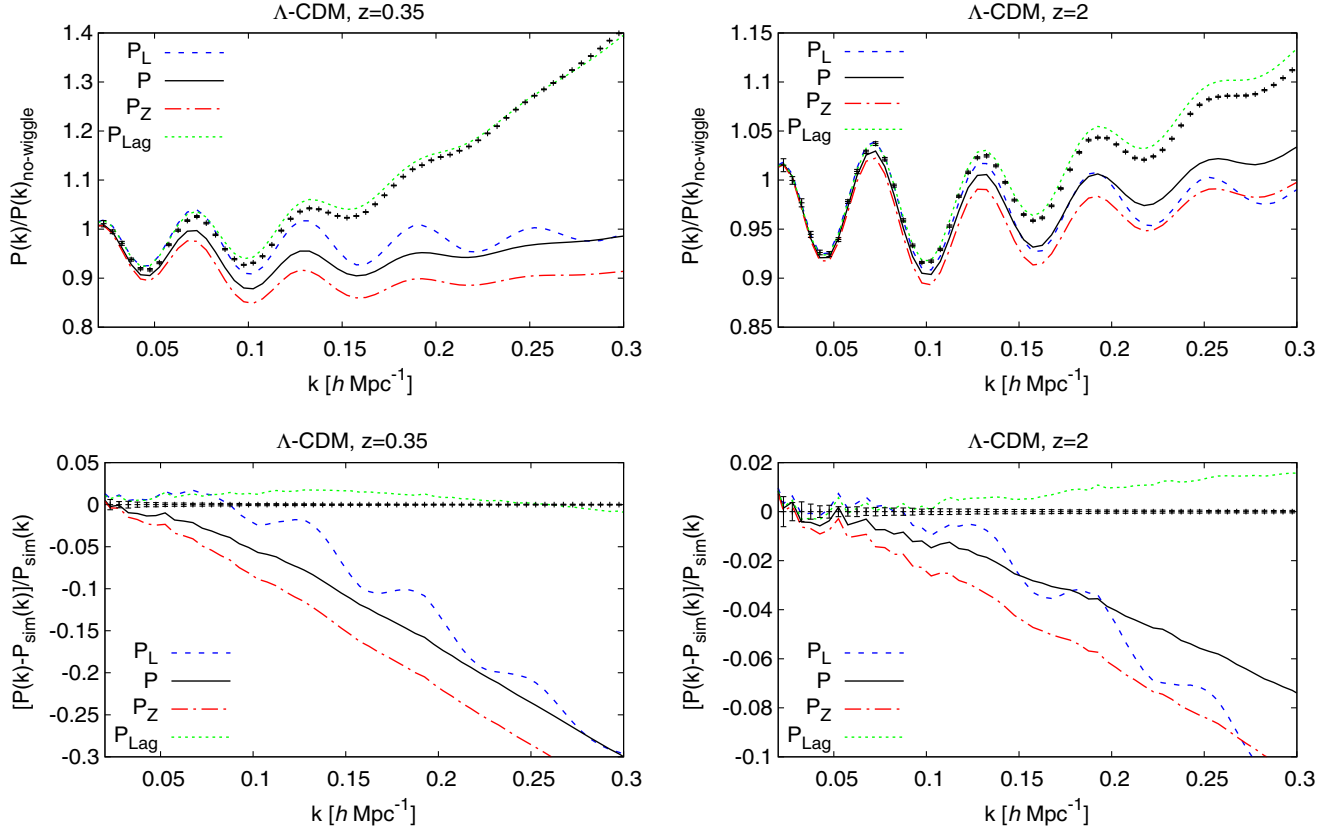
FIG. 13. (Upper) Matter density power spectrum divided by a reference no-wiggle linear power spectrum, at redshifts $z = 0.35$ and $z = 2$. We show the predictions of linear theory P_L (blue dashed line), our nonlinear model P (black solid line), the standard Zeldovich approximation P_Z (red dot-dashed line), a Lagrangian model P_{Lag} (green dotted line), and the numerical simulations (black crosses). (Lower) Relative deviation of these density power spectra from the numerical simulations. The error bars centered on zero are the numerical simulations statistical error bars.

decays as k^{-3}. As for the other statistics, the detailed behavior with redshift reflects the change of the effective index n. At $z = 2$, we find that both Δ^2 and Δ_Z^2 rise above the linear power spectrum Δ_L^2 on weakly nonlinear scales, $k \sim 2h\,\text{Mpc}^{-1}$, whereas at $z = 0$ they remain below Δ_L^2. This agrees with the comparison of Figs. 4 and 8.

C. Comparison with numerical simulations

1. Matter density power spectrum

Finally, we compare the predictions of our curl-free Gaussian *Ansatz* with numerical simulations of the large-scale matter density field in the Λ-CDM cosmology, which were presented in [14,70]. Since our Gaussian model cannot describe highly nonlinear scales, as explained in the previous sections, we focus on large quasilinear scales associated with the baryon acoustic peak. We show the matter density power spectrum in Fig. 13. To distinguish more clearly the baryon acoustic oscillations and the different models, we plot in the upper panels the ratio of the density power spectra by a reference no-wiggle linear power spectrum that does not contain baryon acoustic

oscillations. In the lower panels, we directly plot the relative deviation from the numerical simulations.

As we can see in the upper panels of Fig. 13, our result $P(k)$ is similar to the standard Zeldovich approximation on these large scales. This agrees with the results of Fig. 12 and the fact that on such large scales the effective truncation of the displacement power spectrum on nonlinear scales does not have a great impact. Thus, the damping of the oscillations at higher k, as compared with the linear power spectrum, is similar in both models. However, in agreement with the results of previous sections, the amplitude of the power spectrum given by our model is somewhat larger than for the standard Zeldovich approximation. Thus, the modification of the displacement field on nonlinear scales only leads to a broadband change to the density power spectrum on BAO scales. In agreement with Fig. 12, our power spectrum remains below the linear theory up to $k \leq 0.3h/\text{Mpc}$ at $z = 0.35$, while it raises above the linear theory at $k \simeq 0.2h/\text{Mpc}$ at $z = 2$. In terms of the absolute value of the density power spectrum, our model is not competitive with other approaches that can reach percent-level accuracy on these scales, as shown, for instance, by the comparison with the Lagrangian model $P_{\text{Lag}}(k)$

developed in [62]. Indeed, this older model is correct up to one-loop order, while matching the halo model on highly nonlinear scales, which ensures a reasonably good accuracy. In contrast, as for the standard Zeldovich approximation, the Gaussian model presented in this paper does not match with SPT at one-loop order. This is due to the use of our Gaussian *Ansatz*. To ensure a correct one-loop order, we should extend this Gaussian *Ansatz* and include three-point correlations. This would, in turn, involve additional constraint equations to the system (113)–(115), associated with the evolution of the bispectrum. We leave such an extension to future works.

The lower panels of Fig. 13 show more clearly that, while the relative deviations from the numerical simulations are of the same order of magnitude for the linear theory, our model, and the Zeldovich approximation, the oscillations found for the linear prediction disappear for both our model and the Zeldovich approximation. This is because nonlinear mode couplings damp the initial baryon acoustic oscillations. Therefore, relative to the flatter nonlinear result (given by the numerical simulations), the linear power spectrum shows oscillations at high k. In contrast, the nonlinear damping of the oscillations is well recovered by our model and the Zeldovich approximation, so that the relative deviation is flat. This suggests that both our model and the Zeldovich approximation could be efficiently used to study the BAO features of the density power spectrum. One simply needs to extract the oscillations from the data (e.g., through a high-pass filter), as in [60,71], or to add to the analytical predictions a smooth low-order polynomial, with one or two free parameters, that describes the smooth drift of the amplitude.

2. Matter density correlation function

We next consider the matter density correlation function in Figs. 14 and 15 for the same models and redshifts. It is computed from the power spectra by integrating

$$\xi(x) = 4\pi \int_0^\infty dk k^2 P(k) j_0(kx). \qquad (127)$$

As seen in Fig. 14, on large scales all curves converge to the linear theory. Whereas the Zeldovich approximation gives a constant correlation at low x, because its power spectrum decays faster than k^{-3} at high k, our model gives a logarithmic growth at low x, because its power spectrum decays as k^{-3} at high k. However, neither model nor the Zeldovich approximation can describe highly nonlinear scales associated with virialized halos. In particular, these methods are not competitive as compared with the Lagrangian model of [62].

We focus on the BAO peak in the upper panels of Fig. 15, while in the lower panels we show the relative deviations with respect to numerical simulations, from weakly nonlinear scales up to the BAO scales. The growth of all
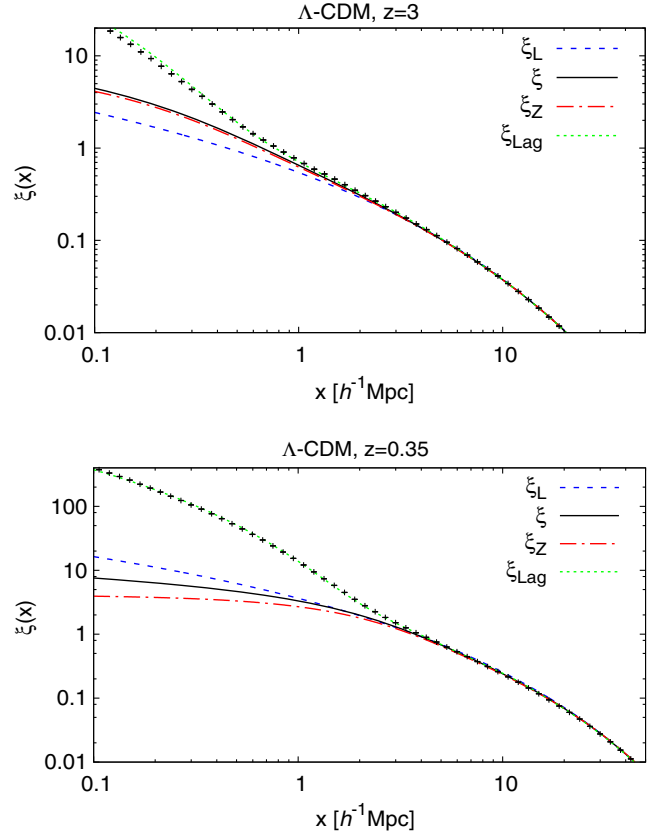

FIG. 14. Matter density correlation function at redshifts $z = 3$ and $z = 0.35$. As in Fig. 13, we show the predictions of linear theory ξ_L (blue dashed line), our nonlinear model ξ (black solid line), the standard Zeldovich approximation ξ_Z (red dot-dashed line), a Lagrangian model ξ_{Lag} (green dotted line), and the numerical simulations (black crosses).

relative deviations and of the simulation error bars at $x \gtrsim 120h^{-1}$ Mpc is due to the fact that the correlation function vanishes at $x \sim 130h^{-1}$ Mpc. Because analytical predictions and numerical simulations do not recover the exact position of this zero crossing, the relative deviation diverges at this point, but this is not a good measure of the validity of approximation schemes.

We recover the fact that the Zeldovich approximation provides a great improvement over the linear prediction for the BAO peak [18,34,72]. Its accuracy is better than 3% accuracy on these scales and redshifts. Our Gaussian model gives similar results, with an improved accuracy below 2% on BAO scales, $70 < x < 120h^{-1}$ Mpc. It actually fares slightly better than the Lagrangian model of [62], which, however, gave a much better prediction for the power spectrum in Fig. 13. In agreement with the discussion above, this means that the information associated with the position and shape of the baryon acoustic peak in the correlation function is related to the frequency and damping of the baryon acoustic oscillations in the power spectrum and is mostly independent of any additional smooth drift. This agrees with the results of Noda *et al.* [60], who also
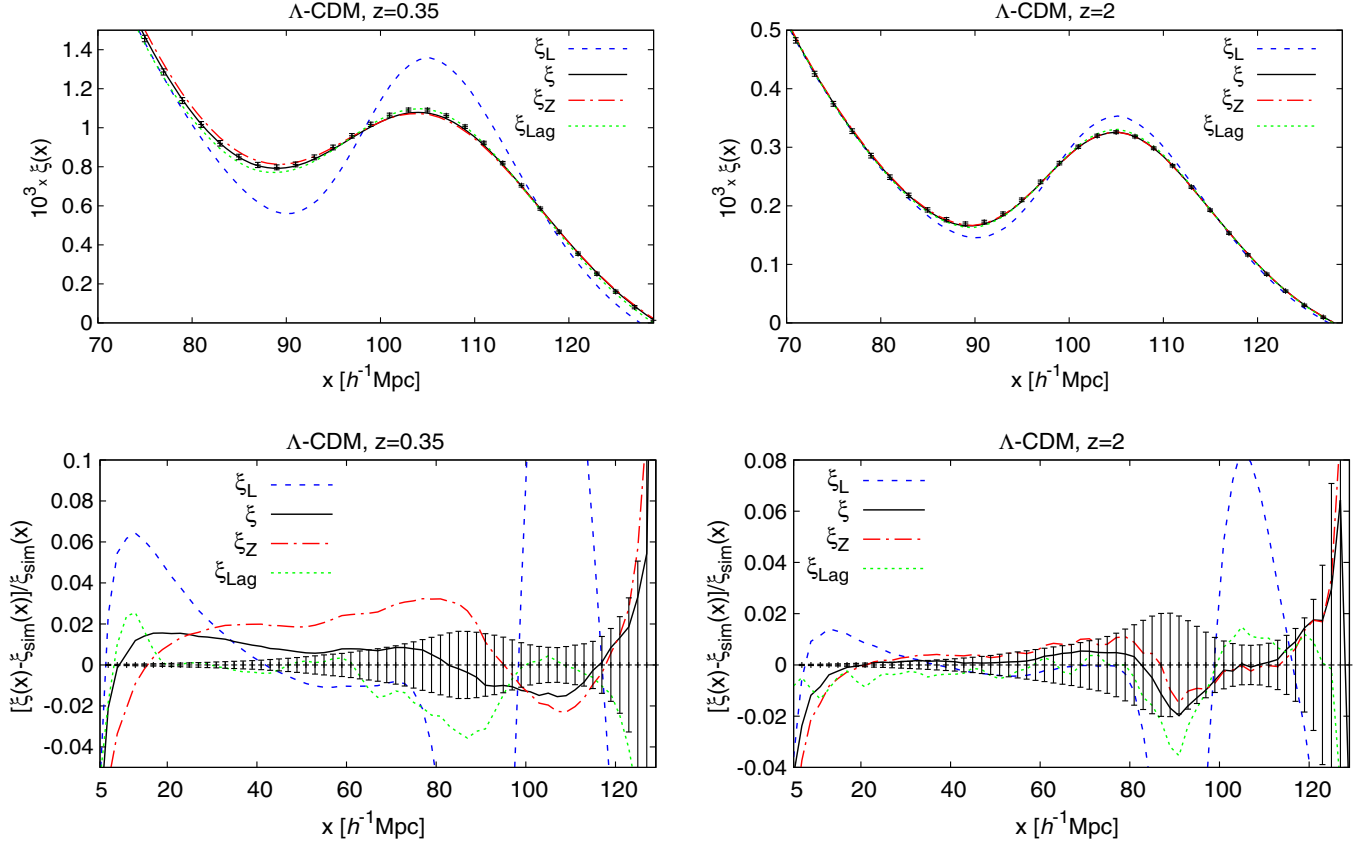
FIG. 15. (Upper) Matter density correlation function at redshifts $z = 0.35$ and $z = 2$. As in Fig. 13, we show the predictions of linear theory ξ_L (blue dashed line), our nonlinear model ξ (black solid line), the standard Zeldovich approximation ξ_Z (red dot-dashed line), a Lagrangian model ξ_{Lag} (green dotted line), and the numerical simulations (black crosses). (Lower) Relative deviation of these density correlation functions from the numerical simulations. The error bars centered on zero are the numerical simulations statistical error bars.

find that the BAO oscillatory features of the power spectrum are mostly governed by the long-range displacements (infrared effects), which are automatically taken into account by Lagrangian approaches, while the broadband shape is affected by small-scale processes (see also [18,73]).

Thus, our model provides the BAO peak of the density correlation function to better than 2%, without any free parameter. Its accuracy is actually the same as that of the numerical simulations. On smaller scales, the Lagrangian model of [62] is usually more accurate, but we find that our model agrees with the numerical simulations to better than 2% down to $7h^{-1}$ Mpc, at $z \geq 0.35$. This level of accuracy is better than most other approaches. Eulerian perturbation schemes, like SPT or EFT, do not give a well-defined correlation function because they predict a power spectrum that grows artificially fast at high k. Lagrangian approaches that go beyond the Zeldovich approximation by including higher-order cumulants, such as convolution Lagrangian perturbation theory, do not significantly improve over the Zeldovich approximation and can become worse below $30h^{-1}$ Mpc [34].

The better agreement with the configuration-space correlation function $\xi(x)$ than with the matter power spectrum

$P(k)$ shows that the former is a more robust statistics in the nonlinear regime [18,74]. Indeed, in contrast with linear scales, where different Fourier modes are uncorrelated, we can expect nonlinear processes that are local in space to generate weaker correlations between different scales in configuration space than in Fourier space. Then, the power spectrum being the Fourier transform of the correlation function, it receives contributions from the correlation function at all scales. The model presented in this paper is also more naturally suited to configuration-space statistics as it is based on the displacement field, hence on a Lagrangian approach, where we follow particle trajectories in spacetime. Indeed, as for the Zeldovich approximation and its extensions to low-order cumulants, it is known that Lagrangian-space formulations are rather efficient for the two-point correlation functions [18,33,34,72].

In Lagrangian approaches that go beyond the Zeldovich approximation by taking into account higher-order cumulants and are exact up to one or two-loop order, it has been found that higher orders can actually worsen the agreement with simulations on intermediate scales and BAO scales at low redshifts [34,72]. This is partly due to the fact that, within such Lagrangian approaches, as in the standard

Zeldovich approximation, particles do not remain trapped inside nonlinear density fluctuations. This free streaming erases small-scale structures and leads to an underestimate of the matter density fluctuations. Adding higher orders in a perturbative manner does not solve this issue and can actually worsen the problem, as the amplitude of the displacement field is further increased on small scales. The systematic better agreement obtained by our approach is due to the effective truncation of the displacement power spectrum at high k. As for the truncated Zeldovich approximation, this partly cures the erasing of nonlinear structures and provides a better model for the large-scale density field [64].

VIII. CONCLUSION

In this paper, we have presented a new approach to model the gravitational dynamics of large-scale structures. The aim is to avoid introducing free parameters, which need to be fitted to numerical simulations, and to go beyond perturbation theory. To do so, we work within a Lagrangian framework. This allows us to use the exact equations of motion, which remain valid beyond shell crossing, if we neglect baryonic effects. Then, we propose to use these equations of motion as constraints on the evolution of the probability distribution functional $\mathcal{P}(\mathbf{\Psi}, \mathbf{v})$ of the displacement and velocity fields. Thus, the approximation only enters at the level of the description of this distribution $\mathcal{P}$.

In this article, we focus on a Gaussian *Ansatz*, but, in principle, we could consider more complex distributions $\mathcal{P}(\mathbf{\Psi}, \mathbf{v})$, which would involve additional parameters in addition to the power spectra (e.g., low-order cumulants). As the *Ansatz* used for $\mathcal{P}$ becomes more complex, one increases the number of constraints derived from the equations of motion of the particles, so as to fully determine $\mathcal{P}$ (e.g., the evolution equations of low-order correlation functions). In this fashion, one can hope to systematically increase the accuracy of the predictions. However, the complexity beyond the Gaussian case may prove difficult for practical computations. We leave this investigation for future works.

This Gaussian *Ansatz* is also of interest by itself, independent of the more general framework outlined above, as it is a simple extension of the Zeldovich approximation that does not require any new free parameter.

Already at the Gaussian level for $\mathcal{P}(\mathbf{\Psi}, \mathbf{v})$, we have found that this approach leads to interesting results. Because we use exact equations of motion (in fact, a subset of the infinite sequence that determines the exact probability distribution), we go beyond perturbation theory. Then, the displacement-field power spectrum becomes damped on nonlinear scales, with a truncation that is not put by hand but arises from the dynamics. In particular, the damping factor $\lambda_\infty \sim e^{-1/(12\alpha_0)}$ is nonperturbative and shows the characteristic exponential factor associated with the probability to form nonlinear structures (for Gaussian initial

conditions). Moreover, in contrast with the Zeldovich approximation, the displacement and velocity power spectra are different.

An interesting feature is that the autopower spectra are automatically positive, as they should be, while cross-power spectra can change sign. This positivity property is not put by hand and appears naturally in our framework, while it is often broken in perturbative schemes. This nice behavior is likely related to the fact that, at each time, the probability distribution $\mathcal{P}$ is well defined and all quantities are exactly computed from this distribution. Thus, they follow from physical particle distributions. This ensures that they do not lead to theoretical inconsistencies (such as negative matter densities or inconsistent higher-order correlations).

We find that, both for self-similar dynamics and the realistic Λ-CDM cosmology, the equations of motion for the displacement and velocity power spectra can be integrated in terms of basic functions $y(k, \eta)$ that describe the amount of damping. This reduction provides explicit expressions that ensure the positivity discussed above and also simplifies the computations.

Already at this Gaussian level, this approach improves over the standard Zeldovich approximation. It generates a self-truncation at high k, so that we obtain a finite prediction even when the standard Zeldovich approximation does not exist, as for linear power spectra with a lot of power at high k, $P_L(k) \propto k^n$ with $n \geq -1$. It also improves over the truncated Zeldovich approximation as the truncation is not put by hand and does not need to be fitted to simulations. In a sense, this method obtains the best Gaussian approximation to the gravitational dynamics, as selected by the equations of motion.

We have first discussed the predictions obtained for self-similar dynamics, to understand how the exponent n of the linear power spectrum affects the results. Then, we have considered the realistic Λ-CDM cosmology. There, the qualitative features can be understood from the change with redshift of the effective exponent n. The comparison with numerical simulations shows that our results are probably not competitive with other methods for the density power spectrum on BAO scales, because of the failure to faithfully recover the smooth amplification of the nonlinear power spectrum. However, the damping of the BAOs is well recovered and the method could be useful if one is able to extract the oscillatory pattern from the data, in the spirit of [60,71]. Alternatively, one can add a couple of free nuisance parameters to the model to take care of this smooth component. The agreement with simulations is much better for the configuration-space correlation function. This is expected, as we use a Lagrangian approach and the Zeldovich approximation is already known to significantly improve over linear theory for these statistics. Our prediction improves somewhat further over the Zeldovich approximation and we obtain an accuracy to better than 2% from BAO scales down to $7h^{-1}$ Mpc at $z \geq 0.35$. Although

some other methods may prove more accurate, the fact that there is no free parameter to be marginalized over could make this approach competitive in terms of constraining power on cosmological scenarios. We leave such an investigation for future works.

Thus, at this stage, the quantitative and practical results of this model are rather modest. However, it was worth performing a detailed investigation to check the power of this Gaussian *Ansatz*, because it is both the simplest realization of the more general method based on the evolution of the distribution $\mathcal{P}(\mathbf{\Psi}, \mathbf{v})$ and a natural parameter-free extension of the Zeldovich approximation. In particular, it is one of the few parameter-free and non-perturbative analytic schemes that have been developed so far, another one being the adhesion model [56] (although one could consider its effective viscosity as a free parameter that is simply set to zero). In few other approaches does the self-damping of initial small-scale power appear from the dynamics without being introduced by hand, through explicit truncation or counterterms. Works in this direction are [37], where there is an explicit truncation scheme but its parameter is internally calibrated from the behavior of the one-loop correction, or [75], where an effective viscosity is explicitly added but may be estimated from the power on nonlinear scales. Our approach does not involve such explicit modifications.

As explained above, the automatic positivity of auto-power spectra is also an encouraging sign. Unfortunately, to go beyond these somewhat academic points and to provide useful quantitative predictions, the results obtained in this paper show that it will be necessary to go beyond the Gaussian *Ansatz*. For instance, we noticed that on small scales the probability distribution of the displacement divergence χ should be strongly skewed, with a high peak at finite positive values and a long tail toward negative values. However, taking into account these features may be a very difficult task. One possibility would be to include a few low-order cumulants, such as the bispectrum, or to add higher-order terms in the probability distribution itself. An alternative would be to consider nonlinear functionals of Gaussian fields. We plan to investigate such issues in future studies.

At a time when numerical simulations are increasingly efficient, analytic methods face strong challenges. Nevertheless, they may still provide useful insight (as shown by the better understanding of the damping of the BAO peak by works in the last 15 years) and also help understand the outcomes of less-studied alternative cosmologies (e.g., different models of dark matter or dark energy, or modified-gravity scenarios) that have not been studied in detail by simulations yet. In particular, scale-dependent linear growing modes do not bring additional complications to this formalism. Our model may also provide estimates of the magnitude of the counterterms introduced in Eulerian EFT schemes, as it computes non-perturbative corrections.

A natural extension of this work would be to consider redshift-space statistics. This will be addressed in a future paper. Another generalization would be to model the large-scale fluctuations of the intergalactic medium associated with the Lyman-α forest. Indeed, they correspond to weakly nonlinear fields that could be within the reach of analytic methods. However, this would require additional parameters, associated, for instance, with the effective equation of state of the gas and its temperature. We plan to investigate this issue in future works.

APPENDIX A: EXPRESSIONS OF $\lambda(k)$ FOR NUMERICAL COMPUTATIONS

For numerical computations, it is convenient to decompose the last exponential in Eq. (59) over its large-q part and the remainder as

$$\lambda(k) = \lambda_0(k) + \lambda_1(k), \tag{A1}$$

with

$$\lambda_0(k) = \int \frac{d\mathbf{q}d\mathbf{k}'}{(2\pi)^3} \frac{(\mathbf{k}' \cdot \mathbf{k})^2}{(k'^2 + \mu^2)k^2} (e^{i\mathbf{k} \cdot \mathbf{q}} - 1)e^{i\mathbf{k}' \cdot \mathbf{q} - \alpha_\infty k'^2} \tag{A2}$$

and

$$\lambda_1(k) = \int \frac{d\mathbf{q}d\mathbf{k}'}{(2\pi)^3} \frac{(\mathbf{k}' \cdot \mathbf{k})^2}{k'^2 k^2} (e^{i\mathbf{k} \cdot \mathbf{q}} - 1)e^{i\mathbf{k}' \cdot \mathbf{q}}$$
$$\times [e^{-\alpha(q)k'^2 - \beta(q)k'^2(\mathbf{k}' \cdot \mathbf{q})^2/(k'q)^2} - e^{-\alpha_\infty k'^2}]. \tag{A3}$$

In Eq. (A3) we have already taken the limit $\mu \to 0$, as it is regular thanks to the vanishing of the last bracket for $k' \to 0$. The integration over $\mathbf{q}$ gives at once for λ_0

$$\lambda_0(k) = e^{-\alpha_\infty k^2}, \tag{A4}$$

where we took the limit $\mu \to 0$ at the end. For λ_1, it is convenient to take the angular average of the expression (A3) over the direction $\mathbf{\Omega}$ of $\mathbf{k}$, taking advantage of the fact that $\lambda_1(k)$ does not depend on $\mathbf{\Omega}$. Using the property

$$\int \frac{d\mathbf{\Omega}}{4\pi} (\mathbf{n} \cdot \mathbf{k}_2)^2 e^{ik_1 \mathbf{n} \cdot \mathbf{q}} = \frac{k_2^2}{3} \left[j_0(k_1 q) + j_2(k_1 q) \right.$$
$$\left. \times \left(1 - 3\left(\frac{\mathbf{k}_2 \cdot \mathbf{q}}{k_2 q}\right)^2 \right) \right] \tag{A5}$$

and integrating next over the angles of $\mathbf{q}$ and $\mathbf{k}'$, we obtain

$$\lambda_1(k) = \frac{2}{3\pi} \int_0^\infty dq dk' q^2 k'^2 \int_0^1 du \cos(k'qu)$$
$$\times [j_0(kq) + j_2(kq)(1 - 3u^2) - 1]$$
$$\times [e^{-\alpha k'^2 - \beta k'^2 u^2} - e^{-\alpha_\infty k'^2}]. \quad (A6)$$

Using the property [76]

$$\int_0^\infty dx \cos(ax) x^2 e^{-p^2 x^2} = \sqrt{\pi} \frac{2p^2 - a^2}{8p^5} e^{-a^2/(4p^2)}, \quad (A7)$$

the integration over k' yields

$$\lambda_1(k) = \frac{1}{12\sqrt{\pi}} \int_0^\infty dq q^2 \int_0^1 du [j_0(kq) - 1 + j_2(kq)$$
$$\times (1 - 3u^2)] \left\{ \frac{2\alpha + (2\beta - q^2)u^2}{(\alpha + \beta u^2)^{5/2}} e^{-q^2 u^2/[4(\alpha + \beta u^2)]} \right.$$
$$\left. - \frac{2\alpha_\infty - q^2 u^2}{\alpha_\infty^{5/2}} e^{-q^2 u^2/(4\alpha_\infty)} \right\}. \quad (A8)$$

Changing variable from u to $t = q^2 u^2/[4(\alpha + \beta u^2)]$, we can integrate over t most factors and we obtain

$$\lambda_1(k) = \int_0^\infty dq \left\{ \frac{j_0(kq) - 1}{6\sqrt{\pi}} q^2 \left[\frac{e^{-q^2/[4(\alpha+\beta)]}}{\alpha\sqrt{\alpha+\beta}} - \frac{e^{-q^2/(4\alpha_\infty)}}{\alpha_\infty^{3/2}} \right] \right.$$
$$+ j_2(kq) \left[\frac{2}{q} \text{Erf}\left(\frac{q}{2\sqrt{\alpha+\beta}} \right) - \frac{2}{q} \text{Erf}\left(\frac{q}{2\sqrt{\alpha_\infty}} \right) \right.$$
$$- \frac{2e^{-q^2/[4(\alpha+\beta)]}}{\sqrt{\pi}\sqrt{\alpha+\beta}} \left(1 + \frac{(2\alpha - \beta)q^2}{12\alpha(\alpha+\beta)} \right) + \frac{2e^{-q^2/(4\alpha_\infty)}}{\sqrt{\pi}\sqrt{\alpha_\infty}}$$
$$\left. \times \left(1 + \frac{q^2}{6\alpha_\infty} \right) - \frac{8\beta}{\sqrt{\pi}q} \int_0^{q^2/[4(\alpha+\beta)]} dt \frac{(1-2t)t^{3/2}e^{-t}}{q^2 - 4\beta t} \right] \right\}, \quad (A9)$$

where $\text{Erf}(x) = \frac{2}{\sqrt{\pi}} \int_0^x dx e^{-x^2}$ is the error function. This can also be written in terms of the complementary error function, $\text{Erfc}(x) = 1 - \text{Erf}(x) = \frac{2}{\sqrt{\pi}} \int_x^\infty dx e^{-x^2}$, as

$$\lambda_1(k) = \int_0^\infty dq \left\{ \frac{j_0(kq) - 1}{6\sqrt{\pi}} q^2 \left[\frac{e^{-q^2/[4(\alpha+\beta)]}}{\alpha\sqrt{\alpha+\beta}} - \frac{e^{-q^2/(4\alpha_\infty)}}{\alpha_\infty^{3/2}} \right] \right.$$
$$+ j_2(kq) \left[-\frac{2}{q} \text{Erfc}\left(\frac{q}{2\sqrt{\alpha+\beta}} \right) + \frac{2}{q} \text{Erfc}\left(\frac{q}{2\sqrt{\alpha_\infty}} \right) \right.$$
$$- \frac{2e^{-q^2/[4(\alpha+\beta)]}}{\sqrt{\pi}\sqrt{\alpha+\beta}} \left(1 + \frac{(2\alpha - \beta)q^2}{12\alpha(\alpha+\beta)} \right) + \frac{2e^{-q^2/(4\alpha_\infty)}}{\sqrt{\pi}\sqrt{\alpha_\infty}}$$
$$\left. \times \left(1 + \frac{q^2}{6\alpha_\infty} \right) - \frac{8\beta}{\sqrt{\pi}q} \int_0^{q^2/[4(\alpha+\beta)]} dt \frac{(1-2t)t^{3/2}e^{-t}}{q^2 - 4\beta t} \right] \right\}. \quad (A10)$$

From Eq. (A10), we can see that $\lambda_1(k) \propto k^2$ at low k, while Eq. (A4) gives $\lambda_0 \to 1$. This gives the large-scale limit (67).

At large k, $\lambda_0(k)$ vanishes while the factors in Eq. (A9) associated with $[j_0(kq) - 1]$, paired with the second term in the following bracket, or with $j_2(kq)$ go to a constant. Then, Eq. (A9) is dominated by the factor $[j_0(kq) - 1]$ associated with the first term in the following bracket. Using the small-scale behaviors (63), we obtain Eq. (68).

For linear density fields with a lot of power on large scales, where $P_L(k)$ grows at least as fast as $1/k$ for $k \to 0$, the variance α_∞ is infinite. This occurs for the self-similar case $n = -2$ studied in Sec. VI C 2. Then, we still perform the decomposition (A1) but α_∞ is now an arbitrary parameter that we take of order $1/k_{\text{NL}}^2$. Indeed, the decomposition (A1) is only used for numerical convenience and the result $\lambda = \lambda_0 + \lambda_1$ does not depend on the choice of α_∞. We checked that our numerical result does not change as we vary α_∞ over 2 orders of magnitude. Then, all expressions above still apply.

APPENDIX B: NUMERICAL COMPUTATION OF THE DENSITY POWER SPECTRUM

1. Case where α_∞ is finite

Following [16], for the numerical computation of the density power spectrum (70), it is convenient to also use the expression obtained by expanding the oscillating part of the exponent in Eq. (70) [77]. Using the one-point variance α_∞ introduced in Eq. (61), this gives

$$P(k) = e^{-\alpha_\infty k^2} \int \frac{d\mathbf{q}}{(2\pi)^3} e^{i\mathbf{k}\cdot\mathbf{q}} \sum_{n=0}^\infty \frac{1}{n!}$$
$$\times \left[\int d\mathbf{k}' P_{\chi\chi}(k') \frac{(\mathbf{k}\cdot\mathbf{k}')^2}{k'^4} e^{i\mathbf{k}'\cdot\mathbf{q}} \right]^n. \quad (B1)$$

In particular, the zeroth-order term vanishes for $k \neq 0$ and the linear and quadratic terms give

$$P(k) = e^{-\alpha_\infty k^2} [P_{\chi\chi}(k) + P_{22}(k) + \ldots], \quad (B2)$$

where the dots stand for terms that are cubic or higher powers in $P_{\chi\chi}(k)$ and

$$P_{22}(k) = \int d\mathbf{k}_1 d\mathbf{k}_2 \delta_D(\mathbf{k}_1 + \mathbf{k}_2 - \mathbf{k}) P_{\chi\chi}(k_1) P_{\chi\chi}(k_2)$$
$$\times \frac{(\mathbf{k}_1 \cdot \mathbf{k})^2 (\mathbf{k}_2 \cdot \mathbf{k})^2}{2k_1^4 k_2^4}. \quad (B3)$$

Then, we subtract the two terms of Eq. (B2) from the expansion (72) to obtain

$$P(k) = e^{-\alpha_\infty k^2}[P_{\chi\chi} + P_{22}] + e^{-\alpha_\infty k^2} \int \frac{dq}{2\pi^2} q^2$$

$$\times \left\{ e^{(\alpha_\infty - \alpha - \beta)k^2} \sum_{\ell=0}^{\infty} \left(\frac{2\beta k}{q} \right)^\ell j_\ell(kq) \right.$$

$$- \left[1 + (\alpha_\infty - \alpha - \beta)k^2 + \frac{1}{2}(\alpha_\infty - \alpha - \beta)^2 k^4 \right] j_0(kq)$$

$$\left. - [1 + (\alpha_\infty - \alpha - \beta)k^2] \frac{2\beta k}{q} j_1(kq) - \left(\frac{2\beta k}{q} \right)^2 j_2(kq) \right\}.$$

(B4)

This ensures that the integral over q is regular and shows a fast convergence at large q.

Here we assumed that α_∞ is finite. In particular, $\beta \to 0$ for $q \to \infty$, so that higher orders in ℓ in the series in Eq. (B4) are strongly suppressed. This corresponds to the power spectrum $n = 0$, in the self-similar case studied in Sec. VI C 1, and to the Λ-CDM cosmology studied in Sec. VII.

2. Case $n = -2$ where α_∞ is infinite

When α_∞ is infinite, as for the case $n = -2$ studied in Sec. VI C 2, we modify the approach leading to Eq. (B4).

Instead of subtracting a term $e^{-\alpha_\infty k^2}[P_{\chi\chi} + P_{22}]$ from expression (71), we simply subtract the Zeldovich power spectrum (73), which has the same form except that the nonlinear variances α and β are replaced by the linear-theory variances α_L and β_L. For $n = -2$, they are given by Eq. (108). Thus, we write

$$P(k) = P_Z(k) + \int \frac{dq}{2\pi^2} q^2 \int_0^1 d\mu \cos(kq\mu)[e^{-(\alpha + \beta\mu^2)k^2}$$

$$- e^{-\pi(1+\mu^2)k^2 q/16}].$$

(B5)

Integrating over the angle cosine μ as for Eq. (72), we obtain

$$P(k) = P_Z(k) + \int \frac{dq}{2\pi^2} q^2 \sum_{\ell=0}^{\infty} j_\ell(kq) \left[e^{-(\alpha+\beta)k^2} \left(\frac{2\beta k}{q} \right)^\ell \right.$$

$$\left. - e^{-\pi k^2 q/8} \left(\frac{\pi k}{8} \right)^\ell \right].$$

(B6)

This again ensures fast numerical computations. The Zeldovich power spectrum part $P_Z(k)$ is easily computed from the analytical expression (110).

[1] D. J. Eisenstein, H.-j. Seo, and M. J. White, Astrophys. J. **664,** 660 (2007).

[2] D. J. Eisenstein, W. Hu, and M. Tegmark, Astrophys. J. **504,** L57 (1998).

[3] D. Munshi, P. Valageas, L. Van Waerbeke, and A. Heavens, Phys. Rep. **462,** 67 (2008).

[4] A. J. Ross *et al.* (BOSS Collaboration), Mon. Not. R. Astron. Soc. **464,** 1168 (2017).

[5] C. Blake *et al.*, Mon. Not. R. Astron. Soc. **418,** 1707 (2011).

[6] P. Martini *et al.* (DESI Collaboration), Proc. SPIE Int. Soc. Opt. Eng. **10702,** 107021F (2018).

[7] R. Laureijs *et al.* (EUCLID Collaboration), arXiv:1110.3193.

[8] P. A. Abell *et al.* (LSST Science and LSST Project), arXiv:0912.0201.

[9] M. H. Goroff, B. Grinstein, S. J. Rey, and M. B. Wise, Astrophys. J. **311,** 6 (1986).

[10] F. Bernardeau, S. Colombi, E. Gaztanaga, and R. Scoccimarro, Phys. Rep. **367,** 1 (2002).

[11] M. Crocce and R. Scoccimarro, Phys. Rev. D **73,** 063519 (2006).

[12] P. Valageas, Astron. Astrophys. **465,** 725 (2007).

[13] F. Bernardeau, M. Crocce, and R. Scoccimarro, Phys. Rev. D **78,** 103521 (2008).

[14] A. Taruya, F. Bernardeau, T. Nishimichi, and S. Codis, Phys. Rev. D **86,** 103528 (2012).

[15] J. Carlson, M. White, and N. Padmanabhan, Phys. Rev. D **80,** 043531 (2009).

[16] P. Valageas, Astron. Astrophys. **526,** A67 (2011).

[17] D. Blas, M. Garny, and T. Konstandin, J. Cosmol. Astropart. Phys. 01 (2014) 010.

[18] P. Valageas, Phys. Rev. D **88,** 083524 (2013).

[19] C. Pichon and F. Bernardeau, Astron. Astrophys. 343, 663 (1999), http://adsabs.harvard.edu/full/1999A%26A...343..663P.

[20] S. Pueblas and R. Scoccimarro, Phys. Rev. D **80,** 043504 (2009).

[21] M. Pietroni, G. Mangano, N. Saviano, and M. Viel, J. Cosmol. Astropart. Phys. 01 (2012) 019.

[22] D. Baumann, A. Nicolis, L. Senatore, and M. Zaldarriaga, J. Cosmol. Astropart. Phys. 07 (2012) 051.

[23] J. J. M. Carrasco, M. P. Hertzberg, and L. Senatore, J. High Energy Phys. 09 (2012) 082.

[24] G. D'Amico, J. Gleyzes, N. Kokron, D. Markovic, L. Senatore, P. Zhang, F. Beutler, and H. Gil-Marín, J. Cosmol. Astropart. Phys. 05 (2020) 005.

[25] L. Senatore, J. Cosmol. Astropart. Phys. 11 (2015) 007.

[26] A. Perko, L. Senatore, E. Jennings, and R. H. Wechsler, arXiv:1610.09321.

[27] M. Lewandowski, A. Perko, and L. Senatore, J. Cosmol. Astropart. Phys. 05 (2015) 019.

[28] Y. B. Zeldovich, Astron. Astrophys. **5,** 84 (1970), http://adsabs.harvard.edu/full/1970A%26A.....5...84Z.

[29] T. Buchert, Mon. Not. R. Astron. Soc. **254,** 729 (1992).
[30] F. R. Bouchet, R. Juszkiewicz, S. Colombi, and R. Pellat, Astrophys. J. **394,** L5 (1992).
[31] T. Buchert and J. Ehlers, Mon. Not. R. Astron. Soc. **264,** 375 (1993).
[32] F. R. Bouchet, S. Colombi, E. Hivon, and R. Juszkiewicz, Astron. Astrophys. **296,** 575 (1995), http://adsabs.harvard.edu/full/1995A%26A...296..575B.
[33] T. Matsubara, Phys. Rev. D **77,** 063530 (2008).
[34] Z. Vlah, U. Seljak, and T. Baldauf, Phys. Rev. D **91,** 023508 (2015).
[35] T. Matsubara, Phys. Rev. D **92,** 023534 (2015).
[36] A. Taruya and S. Colombi, Mon. Not. R. Astron. Soc. **470,** 4858 (2017).
[37] P. McDonald and Z. Vlah, Phys. Rev. D **97,** 023508 (2018).
[38] P. Valageas, Astron. Astrophys. **421,** 23 (2004).
[39] S. Tassev, J. Cosmol. Astropart. Phys. 10 (2011) 022.
[40] L. M. Widrow and N. Kaiser, Astrophys. J. **416,** L71 (1993).
[41] C. Uhlemann, M. Kopp, and T. Haugg, Phys. Rev. D **90,** 023517 (2014).
[42] A. Taruya and T. Hiramatsu, Astrophys. J. **674,** 617 (2008).
[43] M. Pietroni, J. Cosmol. Astropart. Phys. 10 (2008) 036.
[44] S. Anselmi and M. Pietroni, J. Cosmol. Astropart. Phys. 12 (2012) 013.
[45] M. Davis and P. J. E. Peebles, Astrophys. J. Suppl. Ser. **34,** 425 (1977).
[46] D. Blas, M. Garny, M. M. Ivanov, and S. Sibiryakov, J. Cosmol. Astropart. Phys. 07 (2016) 052.
[47] P. Valageas, Astron. Astrophys. **484,** 79 (2008).
[48] M. K. H. Kiessling, Adv. Appl. Math. **31,** 132 (2003).
[49] A. Gabrielli, M. Joyce, and F. Sicard, Phys. Rev. E **80,** 041108 (2009).
[50] A. Gabrielli, M. Joyce, B. Marcos, and F. Sicard, J. Stat. Phys. **141,** 970 (2010).
[51] F. Bernardeau and P. Valageas, Phys. Rev. D **78,** 083503 (2008).
[52] P. Valageas, Phys. Rev. D **89,** 123522 (2014).
[53] A. Kehagias, H. Perrier, and A. Riotto, Mod. Phys. Lett. A **29,** 1450152 (2014).
[54] P. Schneider and M. Bartelmann, Mon. Not. R. Astron. Soc. **273,** 475 (1995).
[55] A. N. Taylor and A. J. S. Hamilton, Mon. Not. R. Astron. Soc. **282,** 767 (1996).

[56] S. Gurbatov, A. Saichev, and S. Shandarin, Mon. Not. R. Astron. Soc. **236,** 385 (1989).
[57] D. Blas, M. Garny, M. M. Ivanov, and S. Sibiryakov, J. Cosmol. Astropart. Phys. 07 (2016) 028.
[58] M. Peloso and M. Pietroni, J. Cosmol. Astropart. Phys. 01 (2017) 056.
[59] L. Senatore and G. Trevisan, J. Cosmol. Astropart. Phys. 05 (2018) 019.
[60] E. Noda, M. Peloso, and M. Pietroni, J. Cosmol. Astropart. Phys. 08 (2017) 007.
[61] P. Valageas, Astron. Astrophys. **476,** 31 (2007).
[62] P. Valageas, T. Nishimichi, and A. Taruya, Phys. Rev. D **87,** 083522 (2013).
[63] A. Cooray and R. K. Sheth, Phys. Rep. **372,** 1 (2002).
[64] P. Coles, A. L. Melott, and S. F. Shandarin, Mon. Not. R. Astron. Soc. **260,** 765 (1993).
[65] P. J. E. Peebles, *The Large-Scale Structure of the Universe* (Princeton University Press, Princeton, NJ, 1980).
[66] A. Polyanin and V. Zaitsev, *Handbook of Ordinary Differential Equations: Exact Solutions, Methods, and Problems* (Chapman and Hall/CRC, London, 2017).
[67] N. Makino, M. Sasaki, and Y. Suto, Phys. Rev. D **46,** 585 (1992).
[68] R. Scoccimarro and J. Frieman, Astrophys. J. **473,** 620 (1996).
[69] R. Scoccimarro, Astrophys. J. **487,** 1 (1997).
[70] P. Valageas and T. Nishimichi, Astron. Astrophys. **527,** A87 (2011).
[71] E. Noda, M. Peloso, and M. Pietroni, Phys. Dark Universe **29,** 100579 (2020).
[72] T. Okamura, A. Taruya, and T. Matsubara, J. Cosmol. Astropart. Phys. 08 (2011) 012.
[73] T. Baldauf, M. Mirbabayi, M. Simonović, and M. Zaldarriaga, Phys. Rev. D **92,** 043514 (2015).
[74] S. Tassev, J. Cosmol. Astropart. Phys. 06 (2014) 008.
[75] D. Blas, S. Floerchinger, M. Garny, N. Tetradis, and U. A. Wiedemann, J. Cosmol. Astropart. Phys. 11 (2015) 049.
[76] I. S. Gradshteyn and I. M. Ryzhik, *Table of Integrals, Series, and Products*, 4th ed. (Academic Press, New York, 1965).
[77] M. Crocce and R. Scoccimarro, Phys. Rev. D **73,** 063520 (2006).